AIMS Mathematics, 10(7): 16498–16525.
DOI: 10.3934/math.2025739
Received: 22 May 2025
Revised: 02 July 2025
Accepted: 09 July 2025
Published: 22 July 2025

https://www.aimspress.com/journal/Math

Research article

Characterizing the physical and dynamical properties of lump, rogue waves and their interactions for a cascaded system with spatio-temporal dispersion and Kerr nonlinearity

Sarfaraz Ahmed[1], **Atef F. Hashem**[2], **Syed T. R. Rizvi**[3] **and Aly R. Seadawy**[4,*]

[1] College of Civil and Transportation Engineering, Shenzhen University, Shenzhen 518060, China

[2] Department of Mathematics and Statistics, College of Science, Imam Mohammad Ibn Saud Islamic University (IMSIU), Riyadh 11432, Saudi Arabia

[3] Department of Mathematics, COMSATS University Islamabad, Lahore Campus, Pakistan

[4] Mathematics Department, Faculty of Science, Taibah University, Al-Madinah Al-Munawarah, 41411, Saudi Arabia

* **Correspondence:** Email: aabdelalim@taibahu.edu.sa.

Abstract: This article uses Hirota's bilinear method (HBM) and appropriate transformations to investigate several lump solution forms in a cascaded system with spatiotemporal dispersion (STD) and Kerr law nonlinearity (KLN). The vector-coupled nonlinear Schrödinger equation is the mathematical model that describes how different solitons propagate through a cascaded system. Using the positive quadratic assumption in bilinear form, we evaluate lump solutions. By using the single and double exponential ansatz in bilinear form, respectively, we additionally investigate lump single-strip and double-strip soliton interactions. Furthermore, by using trigonometric and hyperbolic functions, respectively, we are able to find lump periodic and rogue wave solutions. Additionally, we discuss and illustrate the geometry of our solutions in multiple dimensions, such as contour plots and 3D. We also compute the stability of our solutions.

Keywords: the cascaded system; lump solitons; rogue wave solution; ansatz transformations; Hirota's bilinear method
Mathematics Subject Classification: 35B10, 35C07, 35C08, 35Q35

1. Introduction

Localized electromagnetic waves and solitons play a vital role in the advancement of modern optical communication systems due to their ability to maintain shape and energy over long distances.

The dynamics of solitons in various nonlinear media, such as photonic crystal fibers, metamaterials, polarization-maintaining fibers, and birefringent fibers, have been extensively studied in recent years [1, 2]. Numerous discoveries resulting from these studies have expanded our knowledge of wave propagation and nonlinear interactions in intricate physical settings [3–5]. Rogue waves are localized wave packets with amplitudes noticeably higher than the usual background—have become a major focus of attention among these nonlinear events. The special features of rogue waves in cascaded systems, where several nonlinear and dispersive effects coexist, are crucial for both theoretical study and real-world application. The generation and analytical modeling of rogue waves in such cascaded frameworks are the main topics of this section, which provides important information about their dynamics and possible uses in optical and photonic systems. Rogue waves have attracted a lot of interest because of their destructive effects on coastal and marine buildings [6–8]. They are frequently characterized as uncommon and violent oceanic phenomena. These abruptly occurring waves, which have amplitudes far larger than the surrounding sea state, are dangerous in both natural and artificial settings [9–11]. More complicated nonlinear frameworks, such as cascaded systems with spatio-temporal dispersion and higher-order nonlinearities, have been used in recent years to analyze rogue waves, going beyond conventional hydrodynamic models [12–14]. These cascaded systems provide a rich platform for comprehending the dynamics, stability, and production of rogue waves in actual physical situations because of their nonlinear effects and the interaction of several interacting wave fields [15–17].

In recent years, neural network techniques have become increasingly effective in studying nonlinear partial differential equations because they provide both symbolic interpretability and numerical efficiency [18]. The ability of the bilinear neural network approach to encode bilinear forms, which are essential in integrable systems within deep learning architectures, has drawn attention among scientists [19]. This allows the method to preserve mathematical structure while learning solution patterns. By adding residual connections that improve gradient flow and stability, the bilinear residual network expands on this concept and works well for approximating complex dynamics [20]. Furthermore, the neural network-based symbolic calculation technique bridges the gap between data-driven learning and symbolic computation by using neural models to help find closed-form expressions, symmetries, and conservation laws [21].

Nonlinear media are used to study many types of soliton pulses, including breathers, kink waves, lump waves, rogue waves, multiwaves, solitary, periodic, and their interactions [22–24]. Lump waves (LWs) are distinguished by their localization in all spatial directions and have been observed in a variety of scientific disciplines [25–27]. LWs have a larger propagation energy than regular solitons and are regarded as a limiting form of solitons in some theoretical situations [28–30]. Critical systems, such as those in financial modeling and maritime operations, can be severely and negatively impacted by LWs because of their concentrated energy and potential for abrupt emergence [31–33]. Because of their severe and unexpected character, LW detection and prediction are very important in real-world applications [34–36]. The development of analytical and numerical techniques for the investigation of lump-type solutions has received increasing attention in recent years [37–39]. The lump and rational solutions of nonlinear Schrödinger equations (NLSEs) have become a main interest in recent years [40–42]. Consequently, a number of researchers have developed important techniques to solve NLSEs [43–45]. In this paper, we study the cascaded system given by [48];

$$\begin{cases} iu_t + a_1 u_{xx} + b_1 u_{xt} + c_1|v|^2 u = 0, \\ iv_t + a_2 v_{xx} + b_2 v_{xt} + c_2|u|^2 v + c_3|v|^2 u = 0, \end{cases} \tag{1.1}$$

where the unknown functions $u(x,t)$ and $v(x,t)$ show wave profiles of the two components, and t and x are the temporal and spatial variables. In Eq (1.1), the 1st, 2nd, 3rd, and 4th terms stands for a linear temporal evolution, group velocity-dispersion (GVD), STD, and cross-phase modulation (XPM), successively. While the $c_3|v|^2u$ last term in Eq (1.1) gives the self-phase-modulation (SPM) [46–48]. Here, for $i = 1,\ 2$, a_i, b_i, and c_i denote the parameters of GVD, STD, and XPM, while the term with c_3 gives the SPM [49–51].

Numerous studies examined the governing model; for example, Zhou et al. used the Riccati equation expansion method, the Jacobian expansion strategy, and the Bernoulli equation expansion approach to evaluate dark, bright, and singular optical solitons [48, 52, 53]. Using stabilizing techniques, Zhang et al. calculated source-side series virtual control to enhance the cascaded system [49]. Banaja et al. used an enhanced adomian decomposition approach to work with optical solitons in a cascaded system [50]. Using an expanded trial function method, Sonmezoglu et al. built optical solitons in a cascaded system [51]. For a cascaded system, Raza et al. investigated chaotic, quasi-periodic wave, super nonlinear, periodic solutions, and solitons [52]. The novelty of this study, however, is the computation of localized solutions, such as lump, lump one-strip, lump two-strip, lump periodic, and rogue wave solutions, for cascaded systems with KLN using the proper transformations and HBM. Together with appropriate polynomial functions and HBM, we use logarithmic transformation to generate lump solutions and all other solutions. Every localized solution for Eq (1.1) found using the suggested method is novel and hasn't been reported in any earlier works.

The article for the upcoming sections will be entertained as follows: In Section 2, we will give the description for HBM and their basic operators. In Section 3, we will form a bilinear equation and evaluate the lump solutions in a cascaded system by an appropriate transformations technique. The mixed solution of soliton and lump waves will be in Section 4. A valuable consideration of lump 1-stripe solutions and lump 2-stripe solutions with some suitable profiles will be entertained in Section 4. With the usage of trigonometric ansatz in bilinear equation, we will construct lump periodic solutions in Section 5. By hyperbolic ansatz in bilinear form, we will construct rogue wave solutions in Section 6. In Section 7, we will provide the geometry of solutions, and finally, in Section 8, we will stretch the concluding remarks.

2. Hirota's bilinear method

The standard definition of the Hirota's bilinear operators was first introduced by Hirota [59],

$$D_t^n D_x^m(\alpha.\beta)D = (\frac{\partial}{\partial t} - \frac{\partial}{\partial t'})^n(\frac{\partial}{\partial x} - \frac{\partial}{\partial x'})^m \alpha(x,t)\beta(x',t') \mid x' = x, t' = t'. \tag{2.1}$$

Some bilinear differential operators are given as

$$\begin{aligned} D_x(\alpha.\beta) &= \alpha_x\beta - \alpha\beta_x, \\ D^2x(\alpha.\beta) &= \alpha 2x\beta - 2\alpha_x\beta_x + \alpha\beta_{2x}, \\ D_xD_t(\alpha.\beta) = D_x(\alpha_t\beta - \alpha\beta_t) &= \alpha_{xt} - \alpha_t\beta_x - \alpha_x\beta_t + \alpha\beta_{xt}, \end{aligned}$$

$$D_xD_t(\alpha.\alpha) = 2(\alpha\alpha_{xt} - \alpha_x\alpha_t),$$
$$D_x^4(\alpha.\beta) = \alpha_{4x}\beta - 4\alpha_{3x}\beta_x + 6\alpha_{2x}\beta_{2x} - 4\alpha_x\beta_{3x} + \alpha\beta_{4x},$$
$$D^n(\alpha.\alpha) = 0, \text{ for } n \text{ is odd.} \tag{2.2}$$

3. Lump solution

We take

$$u(x,t) = \frac{g(x,t)}{f(x,t)}, \quad v(x,t) = \frac{g(x,t)}{f(x,t)}, \tag{3.1}$$

where g is complex, while f stands for a real-valued function. By using Eqs (2.1) and (2.2), and Eq (3.1) into Eq (1.1) then we obtain the following Hirota bilinear forms

$$\frac{iD_t(g.f)}{f^2} + \frac{a_1D_x^2(g.f)}{f^2} - \frac{2a_1gD_x^2(f.f)}{f^3} + \frac{b_1D_tD_x(g.f)}{f^2} - \frac{2b_1gD_x(f_t.f)}{f^3} + \frac{c_1g^2g^*}{f^3} = 0, \tag{3.2}$$

and

$$\frac{iD_t(g.f)}{f^2} + \frac{a_2D_x^2(g.f)}{f^2} - \frac{2a_2gD_x^2(f.f)}{f^3} + \frac{b_2D_tD_x(g.f)}{f^2} - \frac{2b_2gD_x(f_t.f)}{f^3} + \frac{c_2g^2g^*}{f^3} + \frac{c_3g^2g^*}{f^3} = 0. \tag{3.3}$$

From Eq (3.2) selecting only terms of f^2 and f^3, then we have the following bilinear forms, respectively:

$$\begin{cases} iD_t(g.f) + a_1D_x^2(g.f) + b_1D_tD_x(g.f) = 0, \\ -2a_1gD_x^2(f.f) - 2b_1gD_x(f_t.f) + c_1g^2g^* = 0. \end{cases} \tag{3.4}$$

Similarly, from Eq (3.3) selecting only terms of f^2 and f^3, then we have the following bilinear forms, respectively:

$$\begin{cases} iD_t(g.f) + a_2D_x^2(g.f) + b_2D_tD_x(g.f) = 0, \\ -2a_2gD_x^2(f.f) - 2b_2gD_x(f_t.f) + c_2g^2g^* + c_3g^2g^* = 0. \end{cases} \tag{3.5}$$

Hirota bilinear Eq (3.4) is equivalent to the following forms, respectively:

$$\begin{cases} i(fg_t - f_tg) + a_1(f_{xx}g - 2f_xg_x + fg_{xx}) + b_1(g_{xt}f - g_xf_t - g_tf_{xx} + gf_{xt}) = 0, \\ -a_1g\left(f_{xx}f - 2f_x^2 + ff_{xx}\right) - 2b_1g(ff_{tx} - f_xf_t) + c_1g^2g^* = 0. \end{cases} \tag{3.6}$$

Similarly, Hirota bilinear Eq (3.5) is equivalent to the following forms, respectively:

$$\begin{cases} i(fg_t - f_tg) + a_2(f_{xx}g - 2f_xg_x + fg_{xx}) + b_2(g_{xt}f - g_xf_t - g_tf_{xx} + gf_{xt}) = 0, \\ -a_2g\left(f_{xx}f - 2f_x^2 + ff_{xx}\right) - 2b_2g(ff_{tx} - f_xf_t) + c_2g^2g^* + c_3g^2g^* = 0. \end{cases} \tag{3.7}$$

For lump solutions of Eq (1.1), we apply the subsequent ansatz in Eqs (3.6) and (3.7) [53–57],

$$g(x,t) = \frac{A_1e^{(ict)}p(x,t)}{q(x,t)}, \quad f(x,t) = 2e^{ict}[\ln q(x,t)]_x, \tag{3.8}$$

where A_1 stands for a non zero constant, while $p(x,t)$ and $q(x,t)$ are unknown functions.

Theorem 1. *In this theorem, we will compute lump solutions to the cascaded system.*

Proof. For finding lump solutions for p and q in Eq (3.8) we use the following hypothesis [54, 55],

$$p = \xi_1^2 + \xi_2^2 + B_2\,, \quad q = \xi_1^2 + \xi_2^2 + B_3, \tag{3.9}$$

where $\xi_1 = B_0x + t$, $\xi_2 = B_1x + t$, and $B_i(1 \le i \le 3)$ are constants. Now using Eq (3.6) to Eq (3.8) and solving the equations obtained from coefficients of x and t gives:
Set I. The values of parameters for Eqs (3.6) and (3.7), respectively,

$$\begin{cases} B_0 = -\frac{1}{b_1c},\ B_2 = -\frac{8\left(-3b_1^2c+3a_1+4c_1\right)}{b_1^2c^3},\ B_3 = \frac{4\left(-3b_1^2c+3a_1+8c_1\right)}{b_1^2c^3},\ B_1 = -\frac{1}{b_1c}, \\ and \\ A_1 = -\frac{\frac{-1}{4}+\frac{i}{4}}{B_1c_3},\ B_0 = iB_1,\ B_3 = 0,\ B_2 = B_2. \end{cases} \tag{3.10}$$

Then values in Eq (3.10) generate LS for Eqs (3.6) and (3.7), respectively,

$$\begin{cases} u(x,t) = \frac{A_1e^{ict}\left(-\frac{8\left(-3b_1^2c+3a_1+4c_1\right)}{b_1^2c^3}+2\left(t-\frac{x}{b_1c}\right)^2\right)}{\frac{4\left(-3b_1^2c+3a_1+8c_1\right)}{b_1^2c^3}+2\left(t-\frac{x}{b_1c}\right)^2}, \\ and \\ v(x,t) = -\frac{8\left(t-\frac{x}{b_1c}\right)}{b_1c\left(\frac{4\left(-3b_1^2c+3a_1+8c_1\right)}{b_1^2c^3}+2\left(t-\frac{x}{b_1c}\right)^2\right)}e^{ict}, \end{cases} \tag{3.11}$$

and

$$\begin{cases} u(x,t) = \frac{\left(\frac{1}{4}-\frac{i}{4}\right)e^{ict}\left(B_2+(t+iB_1x)^2+(t+B_1x)^2\right)}{B_1c_3\left[(t+iB_1x)^2+(t+B_1x)^2\right]}, \\ and \\ v(x,t) = \frac{4iB_1(t+iB_1x)+4B_1(t+B_1x)}{(t+iB_1x)^2+(t+B_1x)^2}e^{ict}. \end{cases} \tag{3.12}$$

Set II. The values of parameters for Eqs (3.6) and (3.7), respectively:

$$\begin{cases} B_2 = \frac{32B_1^2c_1}{c},\ B_1 = B_1,\ B_3 = B_3, \\ and \\ A_1 = -\frac{\left(\frac{i}{4}\right)a_2}{b_2c_3},\ B_0 = -\frac{b_2}{a_2},\ B_1 = -\frac{b_2}{a_2},\ B_2 = 0. \end{cases} \tag{3.13}$$

Then values in Eq (3.13) generate LS for Eqs (3.6) and (3.7), respectively:

$$\begin{cases} u(x,t) = \frac{A_1e^{ict}\left(\frac{32B_1^2c_1}{c}+(t+B_0x)^2+(t+B_1x)^2\right)}{B_1+(t+B_0x)^2+(t+B_1x)^2}, \\ and \\ v(x,t) = \frac{4B_0(t+B_0x)+4B_1(t+B_1x)}{B_3+(t+B_0x)^2+(t+B_1x)^2}e^{ict}, \end{cases} \tag{3.14}$$

and

$$\begin{cases} u(x,t) = -\dfrac{ia_2 e^{ict}\left(t-\frac{b_2 x}{a_2}\right)^2}{2b_2c_3\left(B_3+2\left(t-\frac{b_2 x}{a_2}\right)^2\right)}, \\ and \\ v(x,t) = -\dfrac{8b_2\left(t-\frac{b_2 x}{a_2}\right)}{a_2\left(B_3+2\left(t-\frac{b_2 x}{a_2}\right)^2\right)}e^{ict}. \end{cases} \tag{3.15}$$

To better understand the dynamics of the lump solution $v(x,t)$ governed by Eq (3.11), we present a series of three-dimensional plots under varying values of the parameter B_1. These visualizations illustrate how the structure and intensity of the lump evolve with changes in B_1, while keeping other parameters fixed. Specifically, the figures reveal that for negative values of B_1 (e.g., $B_1 = -10, -8, -5$), the solution exhibits sharper peaks and higher amplitude oscillations, indicating stronger localization and steeper gradients. As B_1 increases toward zero and positive values (e.g., $B_1 = 0, 5$), the wave profile becomes more flattened and broadened, signifying a transition to a smoother, less concentrated lump structure. These plots highlight the sensitivity of the solution to the variation in B_1, offering insight into how the lump's geometry can be tuned via model parameters.

To further illustrate the influence of parameter variation on the lump solution $v(x,t)$ given in Eq (3.11), we present the overhead (top-down) contour views corresponding to the three-dimensional plots shown in Figure 1. These visualizations provide a clearer depiction of the amplitude distribution and structural symmetry of the lump solutions for varying values of B_1. As seen in Figure 2, when B_1 takes on more negative values such as -10 and -8, the contours become more concentrated and elongated, indicating sharper gradients and stronger localization. As B_1 approaches zero and transitions to positive values (e.g., $B_1 = 0, 5$), the contours expand and flatten, showing a dispersion of energy and a broader spatial profile. These overhead views complement the 3D representations by offering an intuitive understanding of how the solution's amplitude and geometry evolve with changes in B_1, reinforcing the sensitivity and tunability of the model.

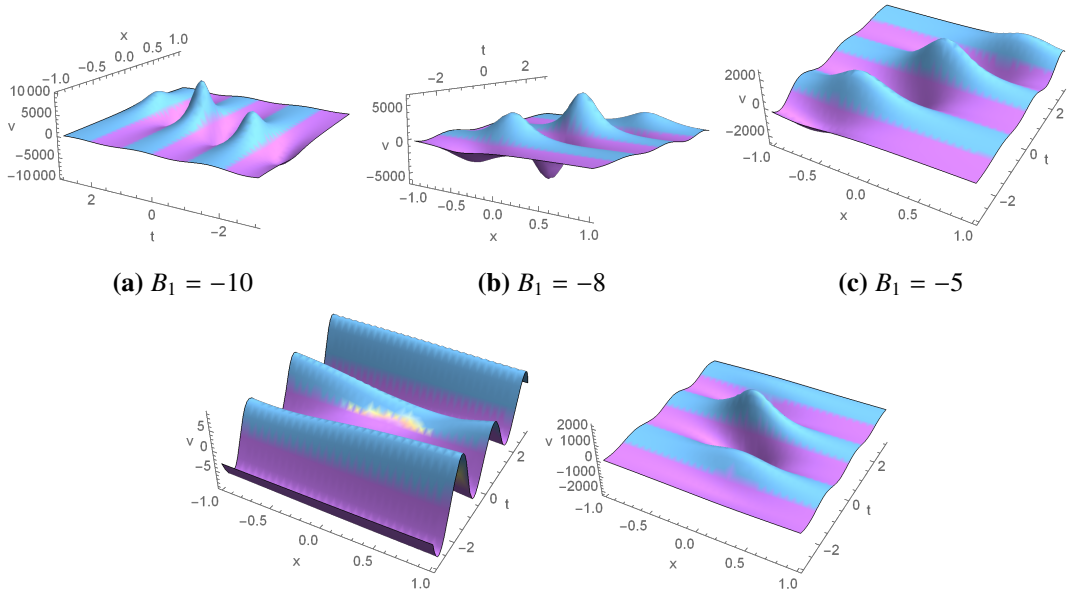

(a) $B_1 = -10$ **(b)** $B_1 = -8$ **(c)** $B_1 = -5$

(d) $B_1 = 0$ **(e)** $B_1 = 5$

Figure 1. Lump solution $v(x,t)$ in Eq (3.11): Perspective interpretation of the LS for $v(x,t)$ with the specific values of parameters $A_1 = 10, B_0 = -2, B_3 = 2, c = 2, c_1 = 2$.

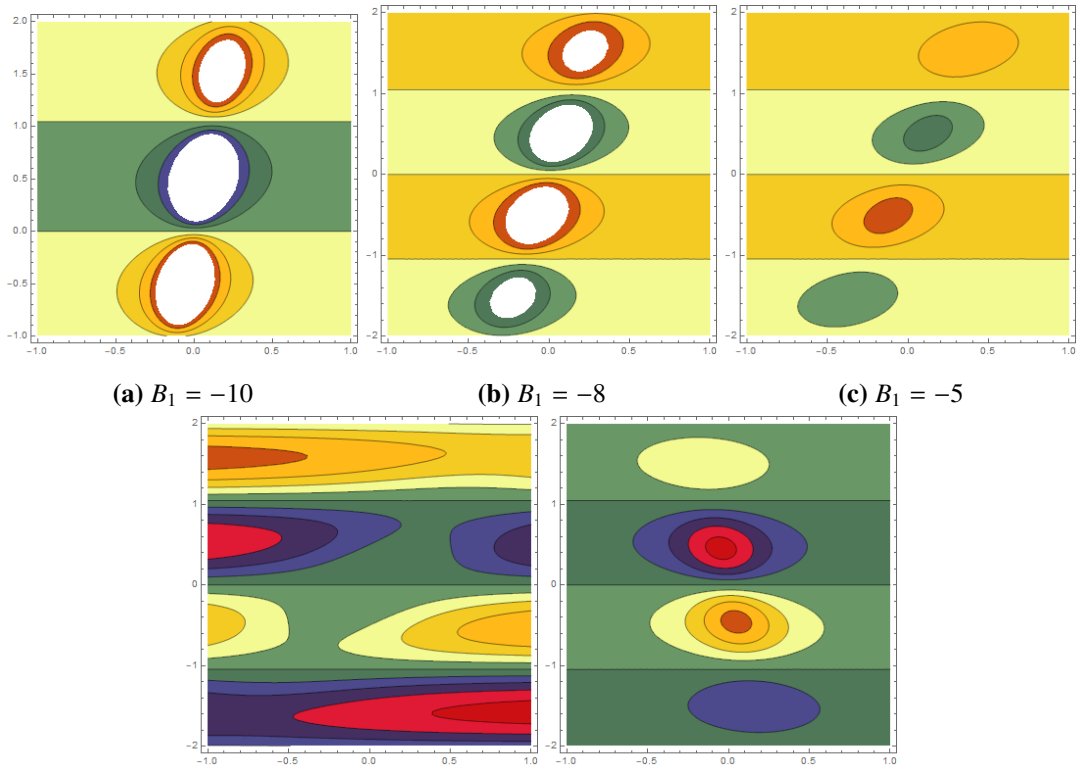

(a) $B_1 = -10$ **(b)** $B_1 = -8$ **(c)** $B_1 = -5$

(d) $B_1 = 0$ **(e)** $B_1 = 5$

Figure 2. Lump solution $v(x,t)$ in Eq (3.11): Overhead view of Figure 1, respectively.

4. Mixed solution of soliton and lump waves

In this section, we will study the interaction of a lump soliton with one kink wave and the interaction of a lump soliton with double kink waves as follows.

4.1. Lump one-strip soliton interaction solution

Theorem 2. *In this theorem, we will compute the lump one-strip soliton interaction solution to the cascaded system.*

Proof. To get lump 1-strip, we apply the following transformation in Eq (3.8) along with Eqs (3.6) and (3.7) [53–57],

$$p = \xi_1^2 + \xi_2^2 + B_2 + b_0 e^{k_1 x + k_2 t}, \quad q = \xi_1^2 + \xi_2^2 + B_3 + b_0 e^{k_1 x + k_2 t}, \tag{4.1}$$

where $\xi_1 = B_0 x + t$, $\xi_2 = B_1 x + t$. The $B_i (1 \le i \le 3)$, k_1, k_2, and b_0 are constants. Now using Eq (4.1) into Eqs (3.6)–(3.8) and extracting coefficients of x, t implies:
Set I. The values of parameters for Eqs (3.6) and (3.7),

$$\begin{cases} B_2 = -\frac{i\left(16B_0^2c_1+16B_1^2c_1+iB_3k_2\right)}{k_2},\ B_1 = B_1,\ B_2 = B_2,\ B_3 = B_3, \\ and \\ B_2 = -\frac{i\left(\frac{-1}{2}+\frac{i}{2}\right)\left(2B_1b_2^3-B_3a_2-iB_3a_2\right)}{b_2^2A_1^2c_2},\ B_0 = -iB_1,\ k_1 = \frac{i}{b_2},\ B_3 = B_3. \end{cases} \tag{4.2}$$

Then values in Eq (4.2) generate required results for Eqs (3.6) and (3.7), respectively:

$$\begin{cases} u(x,t) = \frac{A_1 e^{ict}\left(b_0 e^{k_2 t + k_1 x} - \frac{i\left(16B_0^2c_1+16B_1^2c_1+iB_3k_2\right)}{k_2} + (t+B_0x)^2 + (t+B_1x)^2\right)}{B_3 + b_0 e^{k_2 t + k_1 x} + (t+B_0x)^2 + (t+B_1x)^2}, \\ and \\ v(x,t) = \frac{2\left(b_0 e^{k_2 t + k_1 x} + 2B_0(t+B_0x) + 2B_1(t+B_1x)\right)}{B_3 + b_0 e^{k_2 t + k_1 x} + (t+B_0x)^2 + (t+B_1x)^2} e^{ict}, \end{cases} \tag{4.3}$$

and

$$\begin{cases} u(x,t) = \frac{A_1 e^{ict}\left(-\frac{i\left(\frac{-1}{2}+\frac{i}{2}\right)\left(2B_1b_2^3-B_3a_2-iB_3a_2\right)}{b_2^2A_1^2c_2} + b_0 e^{k_2 t + \frac{i}{b_2}x} + (t-iB_1x)^2 + (t+B_1x)^2\right)}{B_3 + b_0 e^{k_2 t + \frac{i}{b_2}x} + (t-iB_1x)^2 + (t+B_1x)^2}, \\ and \\ v(x,t) = \frac{2\left(\frac{ib_0 e^{k_2 t + \frac{i}{b_2}x}}{b_2} - 2iB_1(t-iB_1x) + 2B_1(t+B_1x)\right)}{B_3 + b_0 e^{k_2 t + \frac{i}{b_2}x} + (t-iB_1x)^2 + (t+B_1x)^2} e^{ict}. \end{cases} \tag{4.4}$$

Set II. The values of parameters for Eqs (3.6) and (3.7), respectively:

$$\begin{cases} B_2 = \frac{B_3(ik_2-4c)}{ik_2+2c}, B_0 = iB_1, k_1 = 0, B_3 = B_3, \\ and \\ B_0 = -\frac{B_3a_2\left(\frac{1}{2}-\frac{i}{2}\right)}{ik_2+2c}, B_1 = \frac{B_3a_2\left(\frac{1}{2}+\frac{i}{2}\right)}{b_2^3}, k_1 = -\frac{i}{b_2}, B_3 = B_3. \end{cases} \tag{4.5}$$

Then values in Eq (4.5) generate required results for Eqs (3.6) and (3.7), respectively:

$$\begin{cases} u(x,t) = \frac{A_1 e^{ict}\left(b_0 e^{k_2 t} + \frac{B_3(ik_2-4c)}{ik_2+2c} + (t+iB_1x)^2 + (t+B_1x)^2\right)}{B_3 + b_0 e^{k_2 t} + (t+iB_1x)^2 + (t+B_1x)^2}, \\ and \\ v(x,t) = \frac{2(2iB_1(t+iB_1x)+2B_1(t+B_1x))}{B_3 + b_0 e^{k_2 t} + (t+iB_1x)^2 + (t+B_1x)^2} e^{ict}, \end{cases} \tag{4.6}$$

and

$$\begin{cases} u(x,t) = \frac{A_1 e^{ict}\left(B_2 + b_0 e^{k_2 t - \frac{ix}{b_2}} + \left(t - \frac{B_3 a_2\left(\frac{1}{2} - \frac{i}{2}\right)}{b_2^3}x\right)^2 + \left(t + \frac{B_3 a_2\left(\frac{1}{2} + \frac{i}{2}\right)}{b_2^3}x\right)^2\right)}{B_3 + b_0 e^{k_2 t - \frac{ix}{b_2}} + \left(t - \frac{B_3 a_2\left(\frac{1}{2} - \frac{i}{2}\right)}{b_2^3}x\right)^2 + \left(t + \frac{B_3 a_2\left(\frac{1}{2} + \frac{i}{2}\right)}{b_2^3}x\right)^2}, \\ and \\ v(x,t) = \frac{2\left(-\frac{ib_0 e^{k_2 t - \frac{ix}{b_2}}}{b_2} - \frac{(1-i)a_2 B_3\left(t - \frac{B_3 a_2\left(\frac{1}{2} - \frac{i}{2}\right)}{b_2^3}x\right)}{b_2^3} + \frac{(1+i)a_2 B_3\left(t + \frac{B_3 a_2\left(\frac{1}{2} + \frac{i}{2}\right)}{b_2^3}x\right)}{b_2^3}\right)}{B_3 + b_0 e^{k_2 t - \frac{ix}{b_2}} + \left(t - \frac{B_3 a_2\left(\frac{1}{2} - \frac{i}{2}\right)}{b_2^3}x\right)^2 + \left(t + \frac{B_3 a_2\left(\frac{1}{2} + \frac{i}{2}\right)}{b_2^3}x\right)^2} e^{ict}. \end{cases} \tag{4.7}$$

Figure 3 illustrates the lump one-strip solution $u(x,t)$ derived from Eq (4.4) for various values of the parameter k_2. As k_2 varies from -10 to 15, the shape and amplitude of the lump-strip structure exhibit noticeable changes. For negative values of k_2, the lump profile is sharp and localized with strong strip-like modulation. As k_2 increases, the structure becomes broader and more flattened, eventually diminishing into a low-amplitude form for higher values such as $k_2 = 15$. These graphical observations demonstrate how k_2 significantly influences the lump-strip dynamics.

Figure 4 presents the contour (overhead) views of the lump one-strip solutions $u(x,t)$ corresponding to Figure 3. The plots depict how the solution profile changes with varying values of the parameter k_2. For lower k_2 values (e.g., $k_2 = -10, -8$), the contours show dense, localized ring structures indicating strong lump features. As k_2 increases toward positive values (e.g., $k_2 = 10, 15$), the lump becomes more diffused and elongated, with the strip pattern gradually smoothing out. These contours highlight the transition from sharp to broader structures as k_2 increases.

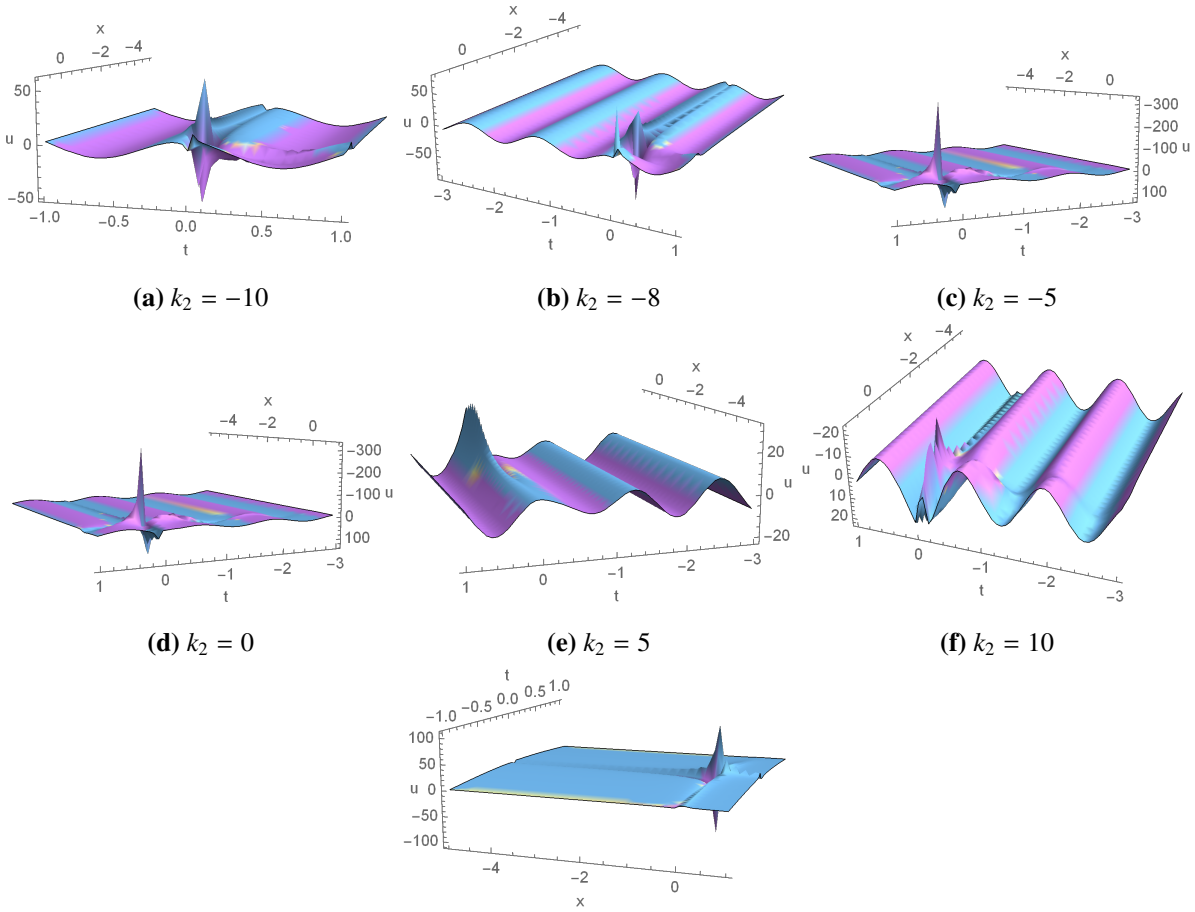

(a) $k_2 = -10$ **(b)** $k_2 = -8$ **(c)** $k_2 = -5$

(d) $k_2 = 0$ **(e)** $k_2 = 5$ **(f)** $k_2 = 10$

(g) $k_2 = 15$

Figure 3. Lump one strip solution $u(x,t)$ in Eq (4.4): Perspective interpretation for $u(x,t)$ with the choice of parameters $A_1 = 10, B_1 = -10, b_0 = -2, b_2 = 4, a_2 = 3, c_2 = 2, c = 5$.

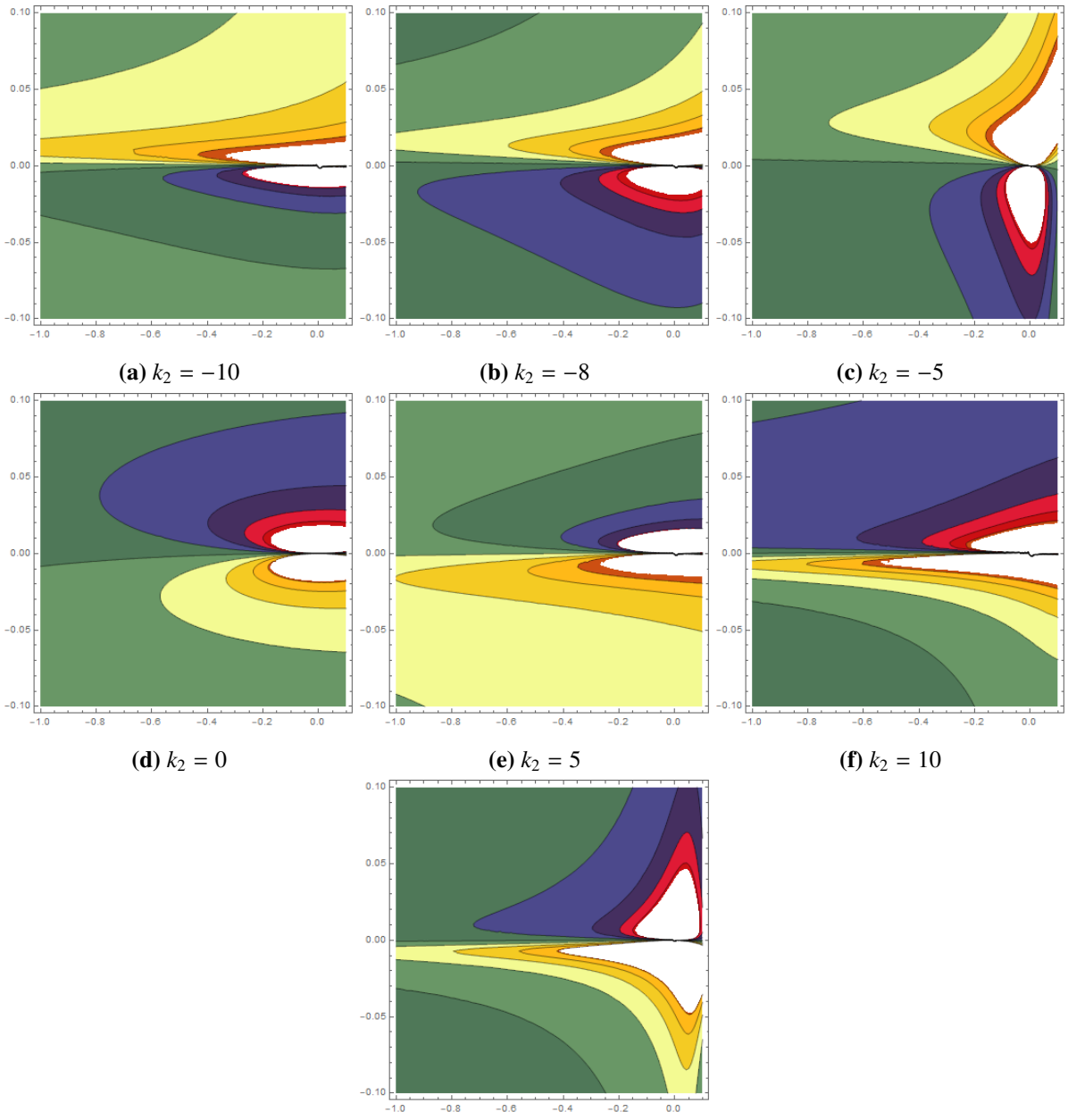

(a) $k_2 = -10$ **(b)** $k_2 = -8$ **(c)** $k_2 = -5$

(d) $k_2 = 0$ **(e)** $k_2 = 5$ **(f)** $k_2 = 10$

(g) $k_2 = 15$

Figure 4. Lump one strip solution $u(x,t)$ in Eq (4.4): Overhead view of Figure 3, respectively.

4.2. Lump double-strip soliton interaction solution

Theorem 3. *In this theorem, we will compute the lump double-strip soliton interaction solution to the cascaded system.*

Proof. To get lump 2-strip, we assume the following transformation [53–57],

$$p = \xi_1^2 + \xi_2^2 + B_3 + m_1 e^{k_1 x + k_2 t + k_3} + m_2 e^{k_1 x + k_2 t + k_3}, \quad q = \xi_1^2 + \xi_2^2 + B_4 + m_1 e^{k_1 x + k_2 t + k_3} + m_2 e^{k_1 x + k_2 t + k_3}, \quad (4.8)$$

where $\xi_1 = B_1x + B_2t$, $\xi_2 = B_1x + B_2t$. While, $B_i(1 \le i \le 4)$, k_1, k_2, k_3, m_1 and m_2 are any specific real parameters. Now using Eq (4.8), Eqs (3.6)–(3.8) and obtaining coefficients of x, t, exp and solving these equations:

Set I. The values of parameters for Eqs (3.6) and (3.8), respectively:

$$\begin{cases} B_2 = -\frac{\frac{1}{3}i\left(6B_1B_3a_1m_2-3B_3^2a_1m_2-6B_1B_3a_1-16B_1B_3c_1+3B_3^2a_1+6cm_2+6c\right)}{m_2-1}, m_1 = \frac{m_2-1}{2}, b_1 = 0, B_3 = B_3, \\ and \\ B_2 = -\frac{i\left(A_1^2c_2k_2k_3m_1+A_1^2c_2k_2k_3m_2+A_1^2c_2k_5k_6m_1+A_1^2c_2k_5k_6m_2-ik_2^2-ik_5^2\right)}{k_5k_6+k_2k_3}, k_1 = -\frac{k_4k_5}{k_2}, b_1 = b_1, B_3 = B_3. \end{cases} \tag{4.9}$$

Then values in Eq (4.9) generates required results for Eqs (3.6) and (3.7), respectively:

$$\begin{cases} u(x,t) = \dfrac{A_1e^{ict}\left(B_3+m_2e^{-\frac{i\left(6B_1B_3a_1m_2-3B_3^2a_1m_2-6B_1B_3a_1-16B_1B_3c_1+3B_3^2a_1+6cm_2+6c\right)}{3m_2-3}+B_1x}+\Omega_1+(k_6+k_5t+k_4x)^2\right)}{B_4+2e^{-\frac{i\left(6B_1B_3a_1m_2-3B_3^2a_1m_2-6B_1B_3a_1-16B_1B_3c_1+3B_3^2a_1+6cm_2+6c\right)}{3m_2-3}+B_1x}+\Omega_2}, \\ \Omega_1 = \left(\frac{1+m_2}{2}\right)e^{-\frac{i\left(6B_1B_3a_1m_2-3B_3^2a_1m_2-6B_1B_3a_1-16B_1B_3c_1+3B_3^2a_1+6cm_2+6c\right)}{3m_2-3}+B_1x}+(k_3+k_2t+k_1x)^2, \\ \Omega_2 = (k_3+k_2t+k_1x)^2+(k_6+k_5t+k_4x)^2, \\ and \\ v(x,t) = \dfrac{2\left(2B_1e^{-\frac{i\left(6B_1B_3a_1m_2-3B_3^2a_1m_2-6B_1B_3a_1-16B_1B_3c_1+3B_3^2a_1+6cm_2+6c\right)}{3m_2-3}+B_1x}+\Omega_3+2k_4(k_6+k_5t+k_4x)\right)}{B_4+2e^{-\frac{i\left(6B_1B_3a_1m_2-3B_3^2a_1m_2-6B_1B_3a_1-16B_1B_3c_1+3B_3^2a_1+6cm_2+6c\right)}{3m_2-3}+B_1x}+\Omega_3}e^{ict}, \\ \Omega_3 = 2k_1(k_3+k_2t+k_1x). \end{cases} \tag{4.10}$$

and

$$\begin{cases} u(x,t) = \dfrac{A_1e^{ict}\left(B_3+m_1e^{-\frac{i\left(A_1^2c_2k_2k_3m_1+A_1^2c_2k_2k_3m_2+A_1^2c_2k_5k_6m_1+A_1^2c_2k_5k_6m_2-ik_2^2-ik_5^2\right)t}{k_5k_6+k_2k_3}+B_1x}+\Omega_4+(k_6+k_5t+k_4x)^2\right)}{B_4+2e^{-\frac{i\left(A_1^2c_2k_2k_3m_1+A_1^2c_2k_2k_3m_2+A_1^2c_2k_5k_6m_1+A_1^2c_2k_5k_6m_2-ik_2^2-ik_5^2\right)t}{k_5k_6+k_2k_3}+B_1x}+\Omega_5}, \\ \Omega_4 = m_2e^{-\frac{i\left(A_1^2c_2k_2k_3m_1+A_1^2c_2k_2k_3m_2+A_1^2c_2k_5k_6m_1+A_1^2c_2k_5k_6m_2-ik_2^2-ik_5^2\right)t}{k_5k_6+k_2k_3}+B_1x}+(k_6+k_5t+k_4x)^2+\left(k_3+k_2t-\frac{k_4k_5}{k_2}x\right)^2, \\ \Omega_5 = (k_6+k_5t+k_4x)^2+\left(k_3+k_2t-\frac{k_4k_5}{k_2}x\right)^2, \\ and \\ v(x,t) = \dfrac{2\left(2B_1e^{-\frac{i\left(A_1^2c_2k_2k_3m_1+A_1^2c_2k_2k_3m_2+A_1^2c_2k_5k_6m_1+A_1^2c_2k_5k_6m_2-ik_2^2-ik_5^2\right)t}{k_5k_6+k_2k_3}+B_1x}+\Omega_6+2k_4(k_6+k_5t+k_4x)\right)}{B_4+2e^{-\frac{i\left(A_1^2c_2k_2k_3m_1+A_1^2c_2k_2k_3m_2+A_1^2c_2k_5k_6m_1+A_1^2c_2k_5k_6m_2-ik_2^2-ik_5^2\right)t}{k_5k_6+k_2k_3}+B_1x}+\Omega_5}e^{ict}, \\ \Omega_6 = -\dfrac{2k_4k_5\left(k_3+k_2t-\frac{k_4k_5}{k_2}x\right)}{k_2}. \end{cases} \tag{4.11}$$

Set II. The values of parameters for Eqs (3.6) and (3.7), respectively:

$$\begin{cases} B_1 = \frac{iB_4m_2-iB_4-2cm_2-2c}{B_4b_1(m_2-1)},\ m_1 = \frac{m_2+1}{2},\ k_1 = k_1,\ B_3 = 0, \\ and \\ A_1 = -\frac{(\frac{2}{3}i)c_3}{b_2c_2},\ B_2 = -\frac{(\frac{4}{9}i)c_3^2(m_1+m_2)}{b_2^2c_2},\ k_1 = -\frac{k_4k_2}{k_5},\ m_1 = m_1. \end{cases} \tag{4.12}$$

Then values in Eq (4.12) generates required results for Eqs (3.6) and (3.7), respectively:

$$\begin{cases} u(x,t) = \dfrac{A_1 e^{ict}\left(m_2 e^{B_2 t+\frac{(iB_4m_2-iB_4-2cm_2-2c)x}{B_4b_1(m_2-1)}} + \frac{1}{2}e^{B_2 x+\frac{(iB_4m_2-iB_4-2cm_2-2c)x}{B_4b_1(m_2-1)}}\left(1+m^2\right)+\Omega_7\right)}{B_4+2e^{B_2 t+\frac{(iB_4m_2-iB_4-2cm_2-2c)x}{B_4b_1(m_2-1)}}+\Omega_7}, \\ \Omega_7 = (k_3+k_2t+k_1x)^2+(k_4+k_5t+k_6x)^2, \\ and v(x,t) = \dfrac{2\left(\frac{2e^{B_2t+\frac{(iB_4m_2-iB_4-2cm_2-2c)x}{B_4b_1(m_2-1)}}}{B_4b_1(m_2-1)}(iB_4m_2-iB_4-2cm_2-2c)+\Omega_8+2k_4(k_6+k_5t+k_4x)\right)}{B_4+2e^{B_2t+\frac{(iB_4m_2-iB_4-2cm_2-2c)x}{B_4b_1(m_2-1)}}+\Omega_7}e^{ict}, \\ \Omega_8 = 2k_1\left(k_3+k_2t+k_1x\right). \end{cases} \tag{4.13}$$

and

$$\begin{cases} u(x,t) = -\dfrac{2ic_3e^{ict}\left(B_3+m_1e^{-\frac{4ic_3^2(m_1+m_2)}{9b_2^2c_2}}+m_2e^{-\frac{4ic_3^2(m_1+m_2)}{9b_2^2c_2}}+\Omega_9+(k_6+k_5t+k_4x)^2\right)}{3b_2c_2\left(B_4+2e^{-\frac{4ic_3^2(m_1+m_2)}{9b_2^2c_2}}+(k_6+k_5t+k_4x)^2+\Omega_9\right)}, \\ \Omega_9 = (k_6+k_5t+k_4x)^2+\left(k_3+k_2t-\frac{k_2k_4}{k_5}x\right)^2, \\ and \\ v(x,t) = -\dfrac{2\left(2B_1e^{-\frac{4ic_3^2(m_1+m_2)}{9b_2^2c_2}+B_1x}+2k_4(k_6+k_5t+k_4x)-\frac{2k_2k_4\left(k_3+k_2t-\frac{k_2k_4x}{k_5}\right)}{k_5}\right)}{B_4+2B_1e^{-\frac{4ic_3^2(m_1+m_2)}{9b_2^2c_2}+B_1x}+(k_6+k_5t+k_4x)^2+\left(k_3+k_2t-\frac{k_2k_4x}{k_5}\right)^2}e^{ict}. \end{cases} \tag{4.14}$$

Figure 5 illustrates the 3D profiles of the lump two-strip solution $u(x,t)$ governed by Eq (4.10) for varying values of the parameter B_1. As B_1 transitions from negative to positive values, we observe significant deformation in the wave structure. For negative B_1 (e.g., $B_1 = -10, -8$), the solution displays multiple sharp spikes aligned in strip formations, indicating high localization and strong nonlinear interactions. As B_1 increases toward positive values (e.g., $B_1 = 10, 15$), the solution evolves into broader humps with smoother and less frequent peaks. The central lump becomes more pronounced, and the surrounding strip waves gradually diminish, demonstrating the sensitivity of the structure to the modulation parameter B_1.

Figure 6 presents the contour plots corresponding to the lump two-strip solution $u(x,t)$ from Figure 5 for various values of B_1. The overhead views clearly display the spatial symmetry and localized wave packets associated with each strip. For negative values of B_1 (e.g., $B_1 = -10, -8$), tightly packed elliptical contours indicate high concentration and dense wave formations along vertical axes. As B_1 increases, the wave interaction region expands and becomes more diffuse, with $B_1 = 5, 10, 15$ exhibiting broader, more separated stripes. These visual patterns confirm the strip-like geometry and demonstrate how B_1 modulates both the number and alignment of wave lobes in the two-strip lump structure.

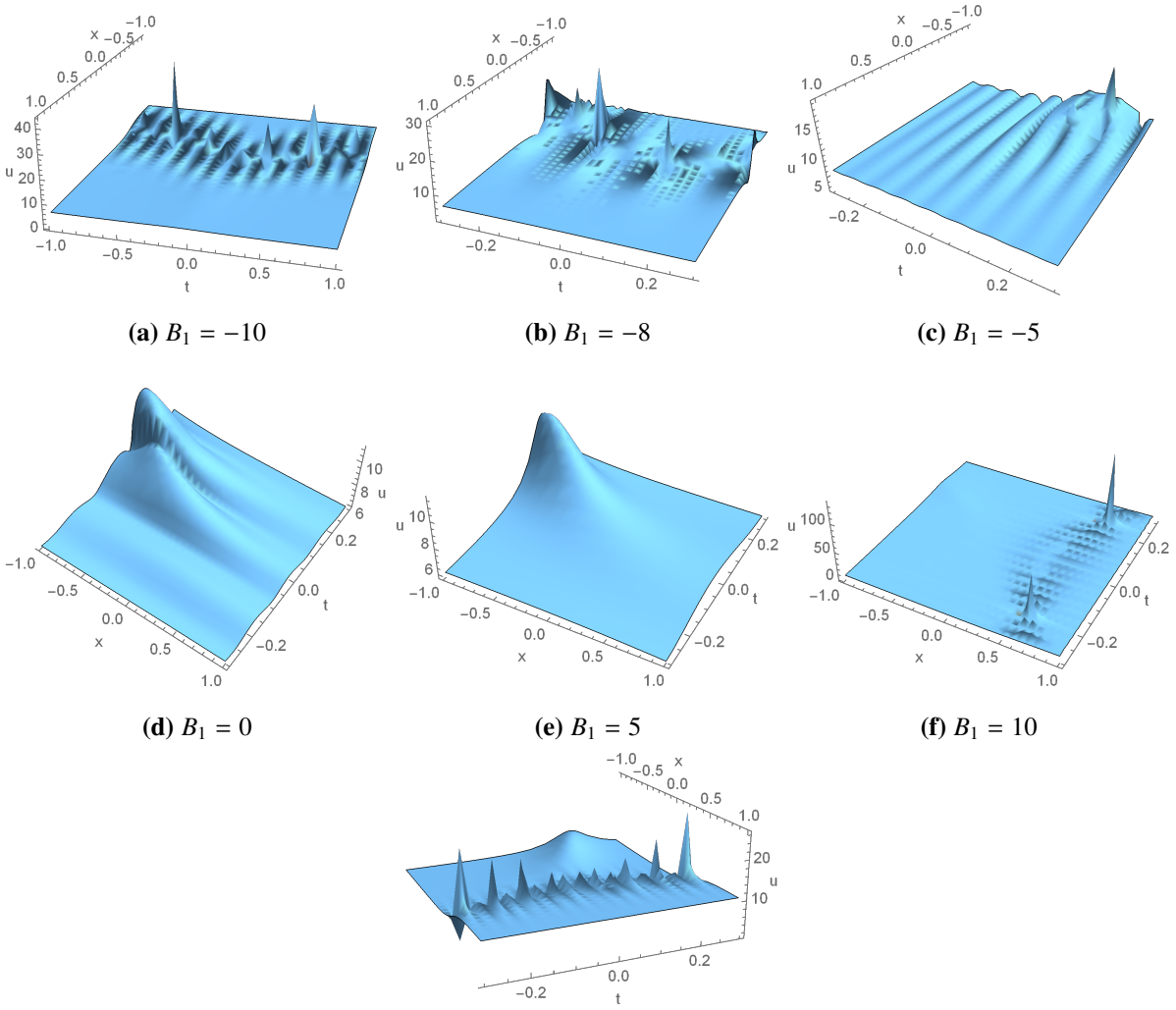

(a) $B_1 = -10$ **(b)** $B_1 = -8$ **(c)** $B_1 = -5$

(d) $B_1 = 0$ **(e)** $B_1 = 5$ **(f)** $B_1 = 10$

(g) $B_1 = 15$

Figure 5. Lump two strip solution $u(x,t)$ in Eq (4.10): Perspective interpretation for $u(x,t)$ with $B_3 = 3, B_4 = 2, a_1 = 3, k_1 = 1, k_2 = 20, k_3 = 5, k_4 = 4, k_5 = 10, k_6 = 2, m_2 = 2, c = 2, c_1 = 2, A_1 = 6$.

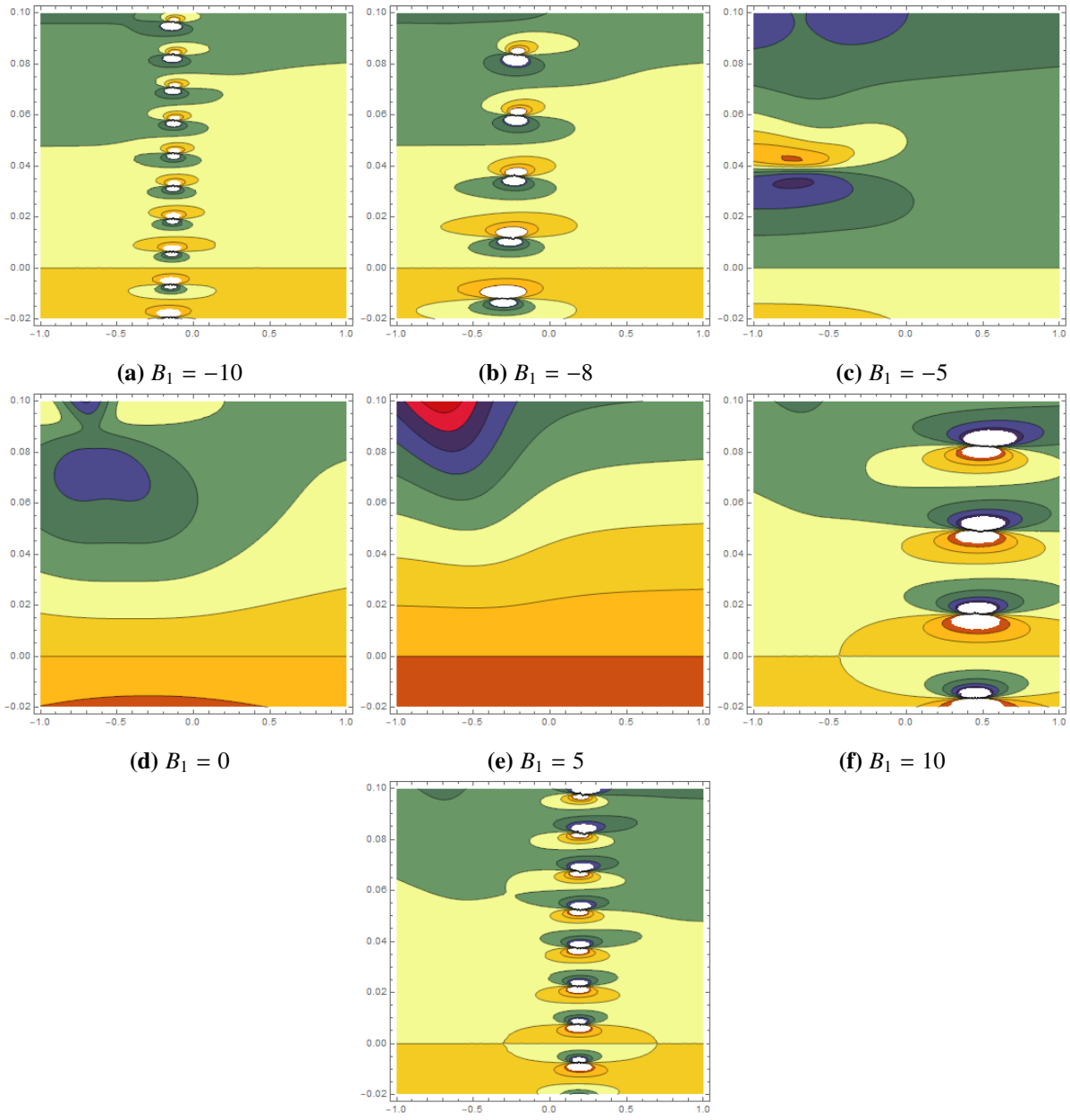

(a) $B_1 = -10$ **(b)** $B_1 = -8$ **(c)** $B_1 = -5$

(d) $B_1 = 0$ **(e)** $B_1 = 5$ **(f)** $B_1 = 10$

(g) $B_1 = 15$

Figure 6. Lump two strip solution $u(x,t)$ in Eq (4.10): Overhead view for $u(x,t)$ with $B_3 = 3, B_4 = 2, a_1 = 3, k_1 = 1, k_2 = 20, k_3 = 5, k_4 = 4, k_5 = 10, k_6 = 2, m_2 = 2, c = 2, c_1 = 2, A_1 = 6$.

5. Lump periodic soliton solution

Theorem 4. *In this theorem, we will compute the lump periodic soliton solution (LPS) to the cascaded system.*

Proof. To compute LPS, we use the following supposition [53–57],

$$p = \xi_1^2 + \xi_2^2 + B_2 + B_3\cos(n_1x + t), \quad q = \xi_1^2 + \xi_2^2 + B_4 + B_5\cos(n_1x + t), \tag{5.1}$$

where $\xi_1 = B_0x + t$, $\xi_2 = B_1x + t$. Whenever $B_i(1 \le i \le 5)$ and n_1 are various parameters to be determined. Now using Eq (5.1) into Eqs (3.6)–(3.8) then letting the coefficients of x, the cos function, and t:

Set I. The values of parameters for Eqs (3.6) and (3.7), respectively:

$$\begin{cases} a_1 = -\frac{2c_1n_2+b_1}{n_2}, n_1 = \frac{b_1^2n_2+\sqrt{8b_1^2c_1^2n_2^4+4b_1^3c_1n_2^3b_1^4n_2^2-8b_1c_1n_2-4b_1^2}}{2b_1(2c_1n_2+b_1)}, c = -\frac{1}{b_1n_2}, B_3 = B_3, \\ and \\ n_2 = \frac{3\left(B_0^3+B_0^2B_1+B_0B_1^2+B_1^3\right)}{4\left(B_0^2+B_0B_1+B_1^2\right)}, b_2 = -\frac{a_2\left(B_0^3+B_0^2B_1+B_0B_1^2+B_1^3\right)}{4\left(B_0^2+B_0B_1+B_1^2\right)}, B_3 = B_3, B_4 = B_4. \end{cases} \tag{5.2}$$

Then values in Eq (5.2) generate required results for Eqs (3.6) and (3.7), respectively:

$$\begin{cases} u(x,t) = \frac{A_1e^{\frac{-it}{b_1n_2}}\left(B_2+(t+B_0x)^2+(t+B_1x)^2+B_4\cos\left[t+\frac{\left(b_1^2n_2+\sqrt{8b_1^2c_1^2n_2^4+4b_1^3c_1n_2^3b_1^4n_2^2-8b_1c_1n_2-4b_1^2}\right)x}{2b_1(2c_1n_2+b_1)}\right]\right)}{B_3+(t+B_0x)^2+(t+B_1x)^2+B_5\cos[t+n_2x]}, \\ and \\ v(x,t) = \frac{2\left[2B_0\left((t+B_0x)^2+2B_1(t+B_1x)^2-B_5n_2sin[t+n_2x]\right)\right]}{B_3+(t+B_0x)^2+(t+B_1x)^2+B_5\cos[t+n_2x]}e^{-i\frac{1}{b_1n_2}t}, \end{cases} \tag{5.3}$$

and

$$\begin{cases} u(x,t) = \frac{A_1e^{\frac{-it}{b_1n_2}}\left(B_2+(t+B_0x)^2+(t+B_1x)^2+B_4\cos[t+n_1x]\right)}{B_3+(t+B_0x)^2+(t+B_1x)^2+B_5\cos\left[t+\frac{3\left(B_0^3+B_0^2B_1+B_0B_1^2+B_1^3\right)x}{4\left(B_0^2+B_0B_1+B_1^2\right)}\right]}, \\ and \\ v(x,t) = \frac{2\left[2B_0\left((t+B_0x)+2B_1(t+B_1x)-\frac{3\left(B_0^3+B_0^2B_1+B_0B_1^2+B_1^3\right)B_5sin\left[t+\frac{3\left(B_0^3+B_0^2B_1+B_0B_1^2+B_1^3\right)x}{4\left(B_0^2+B_0B_1+B_1^2\right)}\right]}{4\left(B_0^2+B_0B_1+B_1^2\right)}\right)\right]}{B_3+(t+B_0x)^2+(t+B_1x)^2+B_5sin\left[t+\frac{3\left(B_0^3+B_0^2B_1+B_0B_1^2+B_1^3\right)x}{4\left(B_0^2+B_0B_1+B_1^2\right)}\right]}e^{ict}. \end{cases} \tag{5.4}$$

Set II. The values of parameters for Eqs (3.6) and (3.7), respectively:

$$\begin{cases} a_1 = -\frac{2c_1n_2+b_1}{n_2}, n_1 = n_1, c = -\frac{1}{b_1n_2}, B_0 = -B_1, B_4 = B_4, \\ and \\ a_1 = a_1, b_2 = 0, n_1 = n_1, c = c, B_0 = -B_1, B_4 = B_4. \end{cases} \tag{5.5}$$

Then values in Eq (5.5) generate required results for Eqs (3.6) and (3.7), respectively:

$$\begin{cases} u(x,t) = \frac{A_1e^{\frac{-it}{b_1n_2}}\left(B_2+(t+B_0x)^2+(t+B_1x)^2+B_4\cos[t+n_1x]\right)}{B_3+(t-B_1x)^2+(t+B_1x)^2+B_5\cos[t+n_1x]}, \\ and \\ v(x,t) = \frac{2\left[-2B_1\left((t-B_1x)^2+2B_1(t+B_1x)^2-B_5n_2sin[t+n_1x]\right)\right]}{B_3+(t-B_1x)^2+(t+B_1x)^2+B_5\cos[t+n_1x]}e^{-i\frac{1}{b_1n_2}t}, \end{cases} \tag{5.6}$$

and

$$\begin{cases} u(x,t) = \frac{A_1 e^{ict}\left(B_2+(t-B_1x)^2+(t+B_1x)^2+B_4\cos[t+n_1x]\right)}{B_3+(t-B_1x)^2+(t+B_1x)^2+B_5\cos[t+n_1x]}, \\ and \\ v(x,t) = \frac{-4B_1\left((t-B_1x)^2+4B_1(t+B_1x)^2-2B_5n_2 sin[t+n_1x]\right)}{B_3+(t-B_1x)^2+(t+B_1x)^2+B_5\cos[t+n_2x]} e^{ict}. \end{cases} \tag{5.7}$$

The 3D and contour plots in Figures 7 and 8 illustrate the lump periodic solution $u(x,t)$ of Eq (5.3) for various values of the parameter B_4. These solutions exhibit an interaction between localized lump structures and periodic wave backgrounds. As B_4 varies from -10 to 15, the solution transitions from dense multi-peak periodic structures to smoother, broader profiles. The surface plots show a periodic wave modulation embedded with localized lump peaks, which become more distinct or diffuse depending on the parameter values. The contour plots reinforce this observation by presenting alternating elliptical ring formations and periodic strip-like bands, clearly indicating the coexistence of periodicity and localization in the wave structure.

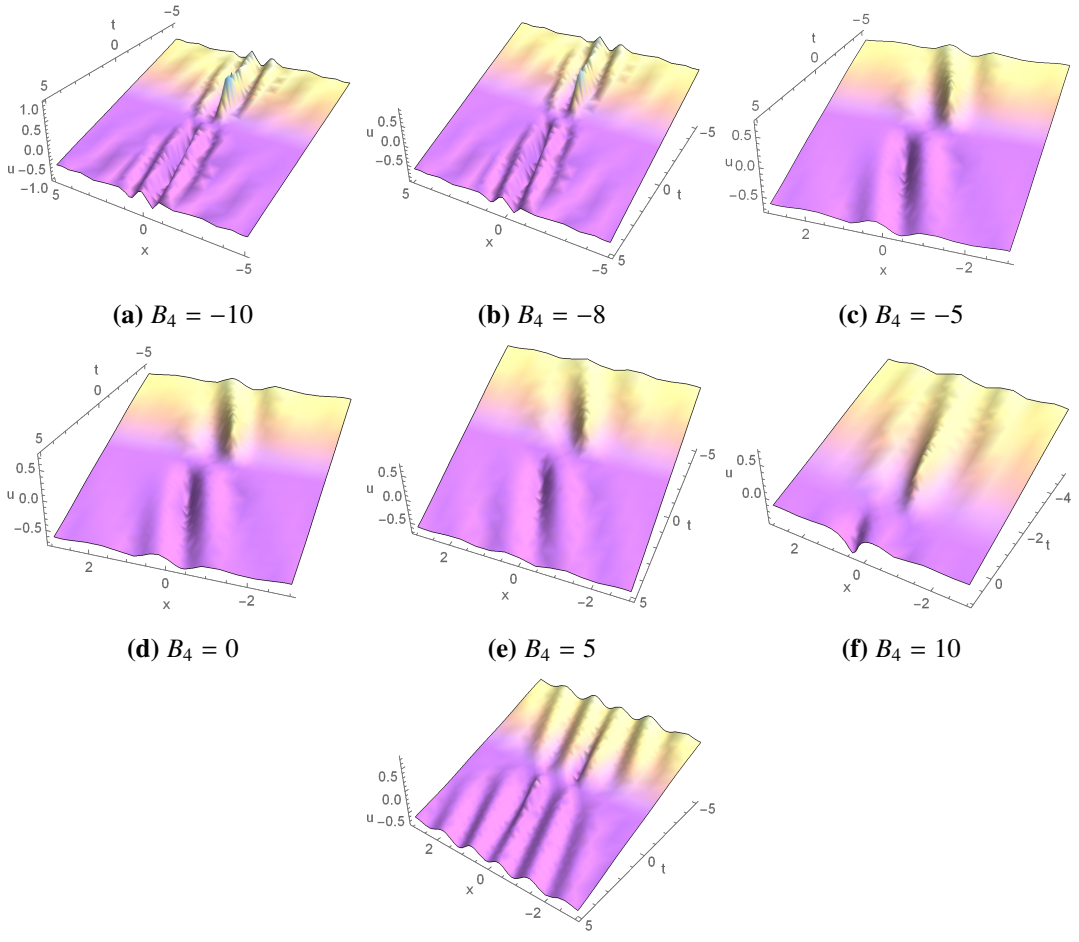

(a) $B_4 = -10$ **(b)** $B_4 = -8$ **(c)** $B_4 = -5$

(d) $B_4 = 0$ **(e)** $B_4 = 5$ **(f)** $B_4 = 10$

(g) $B_4 = 15$

Figure 7. Lump periodic solution $u(x,t)$ in Eq (5.3): Perspective interpretation for $u(x,t)$ with $B_1 = -3, B_2 = 4, B_3 = 2, B_0 = 3, B_5 = 5, b_1 = 20, n_1 = 5, n_2 = 4, c_1 = -1, A_1 = 10$.

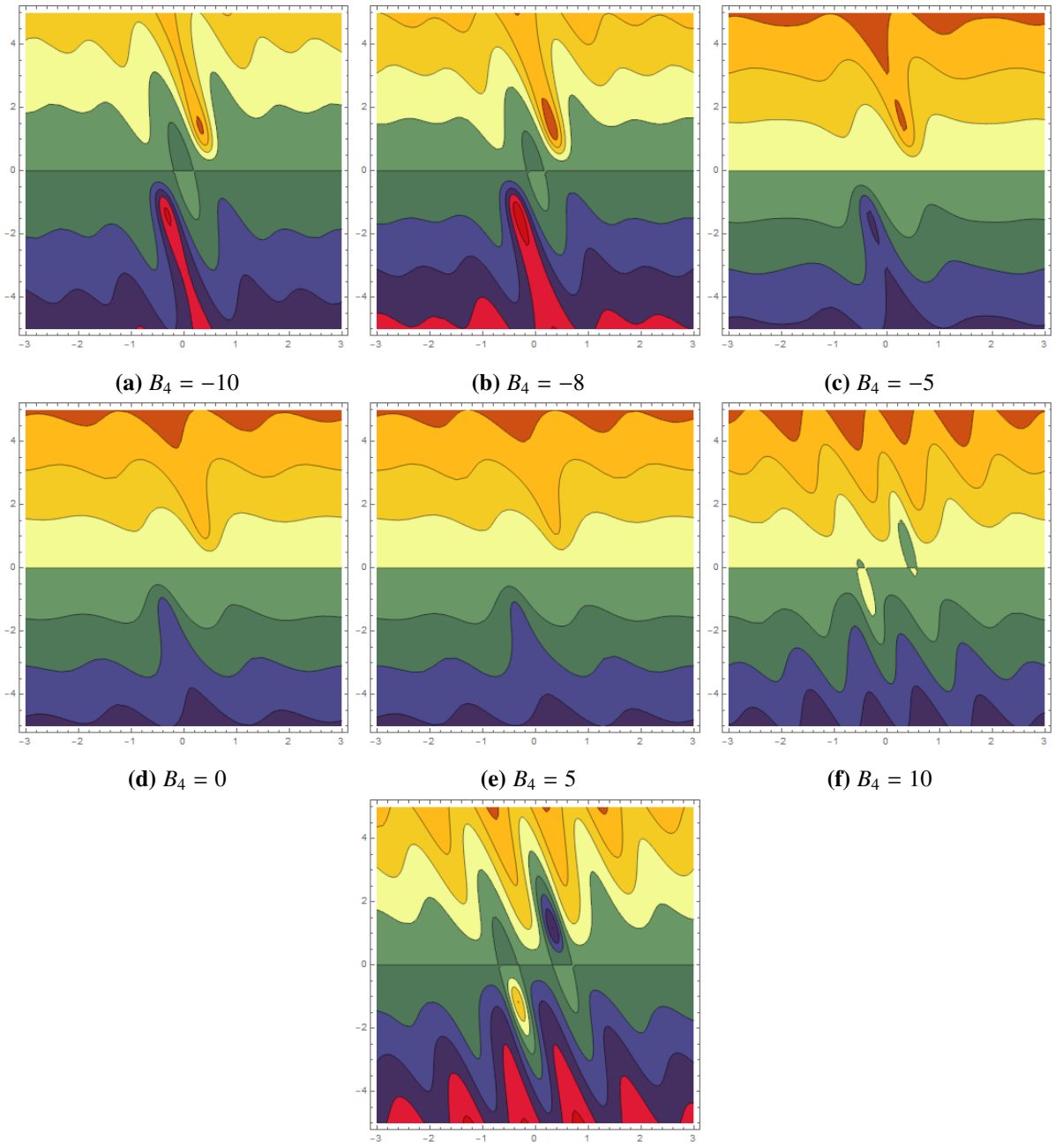

(a) $B_4 = -10$ **(b)** $B_4 = -8$ **(c)** $B_4 = -5$

(d) $B_4 = 0$ **(e)** $B_4 = 5$ **(f)** $B_4 = 10$

(g) $B_4 = 15$

Figure 8. Overhead view for Figure 7, respectively.

6. Rogue wave solutions

Theorem 5. *In this theorem, we will compute the rogue wave solutions (RWS) to the cascaded system.*

Proof. To compute RWS, we use the following supposition [53–57],

$$p = \xi_1^2 + \xi_2^2 + B_2 + B_3 \cosh(n_1 x + t), \quad q = \xi_1^2 + \xi_2^2 + B_4 + B_5 \cosh(n_1 x + t), \tag{6.1}$$

where $\xi_1 = B_0 x + t$, $\xi_2 = B_1 x + t$. Whenever $B_i (1 \leq i \leq 5)$ and n_1 are various parameters to be

determined. Now using Eq (6.1) into Eqs (3.6)–(3.8) then letting the coefficients of x, cos function and t:

Set I. The values of parameters for Eqs (3.6) and (3.7), respectively:

$$\begin{cases} c = \frac{a_1+2c_1}{b_1^2}, n_2 = -\frac{b_1}{a_1+2c_1}, B_4 = 0, B_1 = B_1, \\ and \\ A_1 = \frac{\frac{1}{2}i}{c_3 n_2}, B_4 = 0, n_1 = n_1, c = c, B_0 = B_0. \end{cases} \tag{6.2}$$

Then values in Eq (6.2) generates required results for Eqs (3.6) and (3.7) respectively,

$$\begin{cases} u(x,t) = \frac{A_1 e^{\frac{-i(a_1+2c_1)t}{b_1^2}} \left(B_2+(t+B_0x)^2+(t+B_1x)^2\right)}{B_3+(t-B_1x)^2+(t+B_1x)^2+B_5\cos\left[t-\frac{b_1x}{(a_1+2c_1)}\right]}, \\ and \\ v(x,t) = \frac{2\left[\left(2B_0(t+B_0x)+2B_1(t+B_1x)-\frac{b_1B_5\cos\left[t-\frac{b_1x}{(a_1+2c_1)}\right]}{a_1+2c_1}\right)\right]}{B_3+(t-B_1x)^2+(t+B_1x)^2+B_5\cos\left[t-\frac{b_1x}{(a_1+2c_1)}\right]} e^{i\frac{a_1+2c_1}{b_1^2}t}, \end{cases} \tag{6.3}$$

and

$$\begin{cases} u(x,t) = \frac{ie^{ict}\left(B_2+(t+B_0x)^2+(t+B_1x)^2\right)}{2c_3n_2\left(B_3+(t+B_0x)^2+(t+B_1x)^2+B_5\cosh[t+n_2x]\right)}, \\ and \\ v(x,t) = \frac{2(2B_0(t+B_0x)+2B_1(t+B_1x)+B_5n_2sinh[t+n_2x])}{B_3+(t+B_0x)^2+(t+B_1x)^2+B_5cosh[t+n_2x]} e^{ict}. \end{cases} \tag{6.4}$$

Figure 9 presents both 3D and contour visualizations of the rogue wave solution $v(x,t)$ obtained from Eq (6.3) for varying values of B_5. The 3D plots display a highly localized and sharply peaked wave profile, characteristic of rogue waves that appear suddenly and disappear without a trace. These peaks are centered in space-time and exhibit symmetry about their core. As B_5 changes from -5 to 5, the width and amplitude of the rogue structure vary slightly, but the localized hump and steep descent remain dominant features. The corresponding contour plots show concentric closed curves surrounding the central peak, which visually emphasize the solitary and abrupt nature of the rogue wave, distinguishing it from regular soliton or periodic wave patterns.

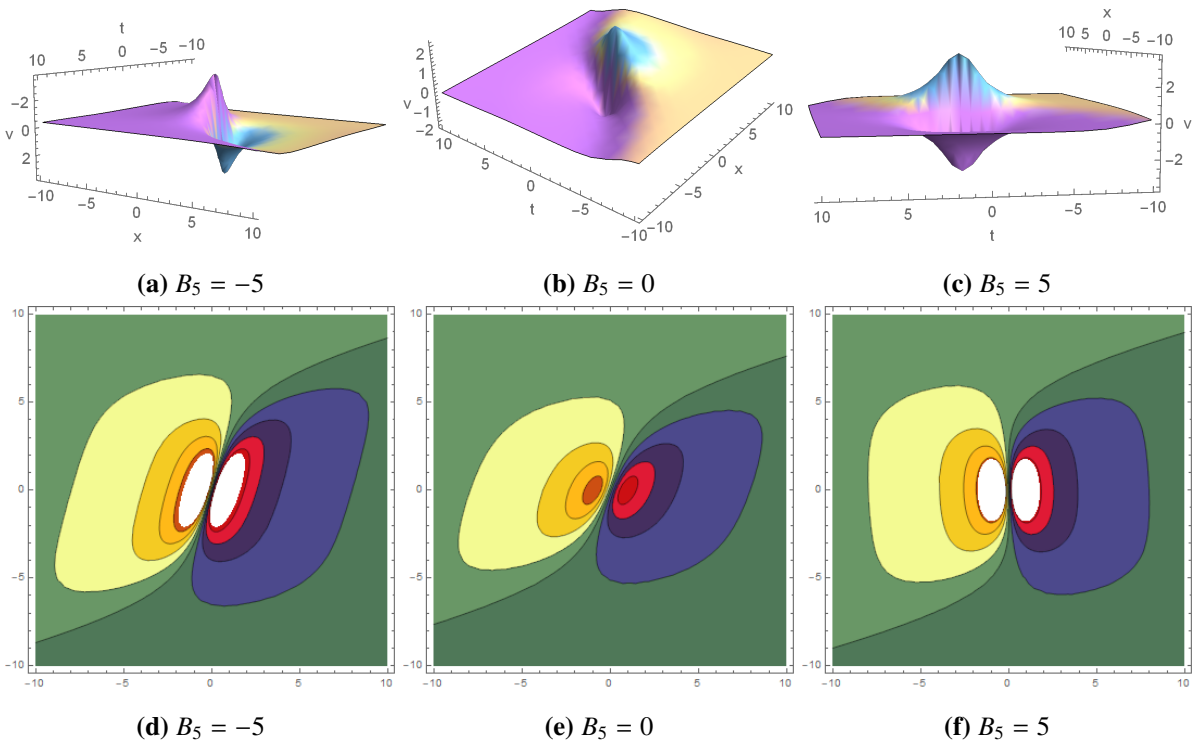

(a) $B_5 = -5$ **(b)** $B_5 = 0$ **(c)** $B_5 = 5$

(d) $B_5 = -5$ **(e)** $B_5 = 0$ **(f)** $B_5 = 5$

Figure 9. Rogue wave solution $v(x,t)$ in Eq (6.3): Perspective and overhead interpretation for $v(x,t)$ with $B_1 = -3, B_0 = -4, B_3 = 2, B_0 = 3, b_1 = 10, a_1 = 50, c_1 = -1$.

7. Stability characteristic of solutions

We compute the stability characteristic for $u(x,t)$ via the Hamiltonian approach [58],

$$u = \frac{1}{2}\int_{-r}^{r} u^2(z)\,dz, \tag{7.1}$$

thus, a stability condition for $u(x,t)$ can be computed as

$$\frac{\partial u}{\partial c} > 0, \tag{7.2}$$

where u denotes the momentum in the Hamiltonian system, and c denotes wave velocity. The stability for $u(x,t)$ in Eq (3.11) via parameters (see Table 1) is given by

$$|\frac{\partial u}{\partial c}|_{c=5} > 0. \tag{7.3}$$

In the interval $x, t \in [-2, 2]$ and $c = 5$, we deduce that u is stable. Similarly, we check out the stability of our solutions; see Table 1.

8. Results and discussion

Table 1 contains all stability properties of our solutions.

Table 1. Stability properties for our solutions.

Solution	Stability	Values of variables.
$u(x,t)$ in Eq (3.11)	Stable	$A_1 = -5, c = 5, c_1 = 2.5, b_1 = 10, a_4 = -9$, and $x, t \in [-2, 2]$.
$v(x,t)$ in Eq (3.11)	Stable	$c_1 = 1.5, c = 5, b_1 = 0.5, a_1 = 1$, and $x, t \in [-2, 2]$.
$u(x,t)$ in Eq (3.12)	Stable	$A_1 = -0.5, B_0 = 4, B_1 = 10, c = 0.1, c_1 = 1, B_3 = 2$, and $x, t \in [-20, 20]$.
$v(x,t)$ in Eq (3.12)	Stable	$B_0 = -6, B_1 = 5, c = 1, c_1 = 10, B_3 = 4.5$, and $x, t \in [-2, 2]$.
$u(x,t)$ in Eq (3.14)	Stable	$A_1 = 3, B_1 = 5.1, c = -5, c_1 = 1, B_0 = 4.5$, and $x, t \in [-2, 2]$.
$v(x,t)$ in Eq (3.14)	Stable	$B_0 = 0.1, B_1 = 5.1, c = -5, c_1 = 1, B_3 = 4.5$, and $x, t \in [-2, 2]$.
$u(x,t)$ in Eq (3.15)	Stable	$a_2 = 0.1, b_2 = 8, c = 5, c_3 = 1, B_3 = 2$, and $x, t \in [-2, 2]$.
$v(x,t)$ in Eq (3.15)	Stable	$a_2 = 1, b_2 = -8, c = 5, c_3 = 1, B_3 = 3$, and $x, t \in [-2, 2]$.
$u(x,t)$ in Eq (4.3)	Stable	$A_1 = 5, c = 5, c_1 = 2.5, b_0 = -3, k_1 = -6, k_2 = -4, B_1 = 0.1, B_0 = -1.5, B_3 = -1$ and $x, t \in [-2, 2]$.
$v(x,t)$ in Eq (4.3)	Stable	$c = -5, c_1 = -2.5, b_0 = 3, k_1 = 6, k_2 = 4, B_1 = 1, B_0 = 1.5, B_3 = 1$ and $x, t \in [-2, 2]$.
$u(x,t)$ in Eq (4.4)	Stable	$A_1 = 1, c = -5, c_1 = 2.5, b_0 = 3.1, k_1 = 6, k_2 = 4, B_1 = 1, B_0 = 1.5, B_3 = 2$ and $x, t \in [-2, 2]$.
$v(x,t)$ in Eq (4.4)	Stable	$c = 5, c_1 = 2.5, b_0 = 3.1, k_1 = 6, k_2 = 4, B_1 = 1, B_0 = 1.5, B_3 = 2$ and $x, t \in [-2, 2]$.
$u(x,t)$ in Eq (4.6)	Stable	$A_1 = 4, c = -5, c_1 = 2.5, c_2 = 3.3, b_0 = 3.1, a_2 = 1, b_2 = 5, k_2 = 4, B_1 = 1, B_0 = 1.5, B_3 = 1$ and $x, t \in [-2, 2]$.
$v(x,t)$ in Eq (4.6)	Stable	$c = -5, c_1 = 2.5, c_2 = 3.3, b_0 = 3.1, a_2 = 1, b_2 = 5, k_2 = 4, B_1 = 1, B_0 = 1.5, B_3 = 1$ and $x, t \in [-2, 2]$.
$u(x,t)$ in Eq (4.7)	Stable	$A_1 = 3, c = -5, c_1 = 2.5, c_2 = 3.3, b_0 = 3.1, a_2 = 1, b_2 = 5, k_2 = 4, B_1 = 1, B_0 = 1.5, B_2 = 8, B_3 = 1$ and $x, t \in [-2, 2]$.
$v(x,t)$ in Eq (4.7)	Stable	$c = -5, c_1 = 2.5, c_2 = 3.3, b_0 = 3.1, a_2 = 1, b_2 = 5, k_2 = 4, B_1 = 1, B_0 = 1.5, B_2 = 8, B_3 = 1$ and $x, t \in [-2, 2]$.
$u(x,t)$ in Eq (4.10)	Stable	$A_1 = -5, c = 5, c_1 = 2.5, k_1 = 1, k_2 = 4, k_3 = 6, k_4 = 2.5, k_5 = 3, k_6 = 2, b_1 = -10, a_1 = -10, B_2 = 4, B_1 = 3, B_3 = 5, B_4 = 10, m_2 = 10$ and $x, t \in [-2, 2]$.
$v(x,t)$ in Eq (4.10)	Stable	$c = 5, c_1 = 2.5, k_1 = 1, k_2 = 4, k_3 = 6, k_4 = 2.5, k_5 = 3, k_6 = 2, b_1 = -10, a_1 = -10, B_2 = 4, B_1 = 3, B_3 = 5, B_4 = 10, m_2 = 10$ and $x, t \in [-2, 2]$.
$u(x,t)$ in Eq (4.11)	Stable	$A_1 = 20, c = 2, c_1 = 2.5, k_1 = 1, k_2 = 4, k_3 = 6, k_4 = 2.5, k_5 = -3, k_6 = -2, b_1 = 10, a_1 = 10, B_2 = 4, B_1 = 1, B_2 = 4, B_3 = 5, B_4 = -9, m_2 = 10$ and $x, t \in [-2, 2]$.
$v(x,t)$ in Eq (4.11)	Stable	$c = 5, c_1 = 2.5, k_1 = 1, k_2 = 4, k_3 = 6, k_4 = 2.5, k_5 = 3, k_6 = 2, b_1 = -10, a_1 = -10, B_2 = 4, B_1 = 3, B_3 = 5, B_4 = 10, m_2 = 10$ and $x, t \in [-2, 2]$.
$u(x,t)$ in Eq (4.13)	Stable	$A_1 = 3, c = 20, c_1 = 5, k_1 = 1, k_2 = 4, k_3 = 6, k_4 = 2.5, k_5 = 3, k_6 = -2, b_1 = 10, a_1 = 5, B_2 = 20, B_1 = 15, B_2 = 20, B_3 = 15, B_4 = 9, m_2 = 10$ and $x, t \in [-2, 2]$.
$v(x,t)$ in Eq (4.13)	Stable	$c = 20, c_1 = 5, k_1 = 1, k_2 = 4, k_3 = 6, k_4 = 2.5, k_5 = 3, k_6 = -2, b_1 = 10, a_1 = 5, B_2 = 20, B_1 = 15, B_2 = 20, B_3 = 15, B_4 = 9, m_2 = 10$ and $x, t \in [-2, 2]$.
$u(x,t)$ in Eq (4.14)	Stable	$A_1 = 3, c = -2.1, c_1 = 10, c_2 = 2.1, c_3 = -4, k_1 = -1, k_2 = 4, k_3 = -6, k_4 = 2.5, k_5 = 3, k_6 = -2, b_1 = 10, b_2 = 3, a_1 = 5, B_2 = -20, B_1 = -15, B_3 = -15, B_4 = -9, m_2 = -10, m_1 = -5$ and $x, t \in [-2, 2]$.
$v(x,t)$ in Eq (4.14)	Stable	$c = 2, c_3 = -4, k_1 = 1, k_2 = 4, k_3 = -6, k_4 = 2.5, k_5 = 3, k_6 = 2, b_2 = 3, a_1 = 5, B_2 = 20, B_1 = 15, B_2 = 20, B_4 = 9, m_2 = 10, m_1 = 5$ and $x, t \in [-2, 2]$.
$u(x,t)$ in Eq (5.3)	Stable	$A_1 = -4, c = 2, c_1 = 3, c_2 = -4, n_1 = 1, n_2 = 4, b_1 = 3, B_0 = 5, B_2 = 2, B_1 = 15, B_4 = 9, B_5 = 2, B_3 = 2.5$, and $x, t \in [-2, 2]$.
$v(x,t)$ in Eq (5.3)	Stable	$c = 2, c_1 = 3, c_2 = -4, n_1 = 1, n_2 = 4, b_1 = 3, B_0 = 5, B_2 = 2, B_1 = 15, B_4 = 9, B_5 = 2, B_3 = 2.5$, and $x, t \in [-2, 2]$..
$u(x,t)$ in Eq (5.4)	Stable	$A_1 = 5, c = 6, c_1 = -3, c_2 = -4, n_1 = 1, b_1 = 3, B_0 = 5, B_2 = 2, B_1 = 15, B_4 = 9, B_5 = 2, B_3 = 2.5$, and $x, t \in [-2, 2]$.
$v(x,t)$ in Eq (5.4)	Stable	$c = 6, c_1 = -3, c_2 = -4, n_1 = 1, b_1 = 3, B_0 = 5, B_2 = 2, B_1 = 15, B_4 = 9, B_5 = 2, B_3 = 2.5$, and $x, t \in [-2, 2]$.
$u(x,t)$ in Eq (5.5)	Stable	$A_1 = -4, c = 2, c_1 = 3, c_2 = -4, n_1 = 1, n_2 = 4, b_1 = 3, B_0 = 5, B_2 = 2, B_1 = 15, B_4 = 9, B_5 = 2, B_3 = 2.5$, and $x, t \in [-2, 2]$.
$v(x,t)$ in Eq (5.5)	Stable	$c = 2, c_1 = 3, c_2 = -4, n_1 = 1, n_2 = 4, b_1 = 3, B_0 = 5, B_2 = 2, B_1 = 15, B_4 = 9, B_5 = 2, B_3 = 2.5$, and $x, t \in [-2, 2]$.
$u(x,t)$ in Eq (5.6)	Stable	$A_1 = -4, c = 2, c_1 = 3, c_2 = -4, n_1 = 1, n_2 = 4, b_1 = 3, B_0 = 5, B_2 = 2, B_1 = 15, B_4 = 9, B_5 = 2, B_3 = 2.5$, and $x, t \in [-2, 2]$.
$v(x,t)$ in Eq (5.6)	Stable	$c = 2, c_1 = 3, c_2 = -4, n_1 = 1, n_2 = 4, b_1 = 3, B_0 = 5, B_2 = 2, B_1 = 15, B_4 = 9, B_5 = 2, B_3 = 2.5$, and $x, t \in [-2, 2]$.

We can see that the solution in Eq (3.11) forms two lump-waves (LW), known as upper bright and lower dark LW, and the bright and dark LWs are symmetrical about the coordinate plane. The solution is called the dark-bright lump solution because the depth of the valley bottom is equal to the height of the peak. When B_1 is changing from the minimum to the maximum number, two-LWs will be altering counterclockwise. When $B_1 = 0$, then LW disappears, but at $B_1 = 5$, the LW gradually appears; see Figure 1. LWs are theoretically viewed as a limit form of soliton in some ways and move with higher propagating energy than general solitons. Consequently, LWs would be destructive, sometimes, be terrible for certain systems, such as in ocean and finance. It is noteworthy to be able to find and anticipate LWs in applications. The valley at the minimum point and peak at the maximum point for the lump solution are symmetric w.r.t the center $(0, 0)$, as shown in Figures 1 and 2. The perspective interpretation of the LS for $v(x, t)$ in Eq (3.11) with the specific values of parameters $A_1 = 10, B_0 = -2, B_3 = 2, c = 2, c_1 = 2$. The overhead view of Figure 1 is displayed in Figure 2, respectively. The perspective interpretation and twisting behaviour of lump one-strip soliton for $u(x, t)$ in Eq (4.4) with the choice of parameters $A_1 = 10, B_1 = -10, b_0 = -2, b_2 = 4, a_2 = 3, c_2 = 2, c = 5$ is displayed in Figure 3. The above two phenomena are matches to fission and fusion phenomena, which occurred among the progress of the lump wave and one stripe wave collisions via appropriate parameters. The two lump-waves (LWs), known as the upper bright and lower dark LWs comes closer and merge into a single lump with the upper bright wave at $k_2 = 0$ (see Figure 3), and for increasing value of k_2, the wave retains its shape. The five lump-waves (LWs), known as, upper bright LWs, comes closer, and after interacting with one another, merge into a single lump with an upper bright wave at $B_1 = 0$ (see Figure 5), and for increasing values of B_1, the LWs retain their shape. The Overhead view of Figure 3 is displayed in Figure 4, respectively. The perspective interpretation and twisting behaviour of the lump double strip soliton for $u(x, t)$ in Eq (4.11) with the selection of parameters $B_3 = 3, B_4 = 2, a_1 = 3, k_1 = 1, k_2 = 20, k_3 = 5, k_4 = 4, k_5 = 10, k_6 = 2, m_2 = 2, c = 2, c_1 = 2, A_1 = 6$ is displayed in Figure 5. The Overhead view of Figure 5 is displayed in Figure 6, respectively. The lump periodic soliton $u(x, t)$ in Eq (5.3) is attained with suitable values of $B_1 = -3, B_2 = 4, B_3 = 2, B_0 = 3, B_5 = 5, b_1 = 20, n_1 = 5, n_2 = 4, c_1 = -1, A_1 = 10$. When B_1 is changing from -10 to 15, the lump periodic (LP) wave will be altering and its behaviour can be seen in Figure 7. When $B_1 = 0$, then the amplitude for the LP wave decreases, but at $B_1 = 15$, the amplitude for the LP wave gradually increases, see Figure 7. The Overhead view of Figure 7 is displayed in Figure 8, respectively. When B_5 is changing from -5 to 10, the rogue wave will be altering, and its behavior can be seen in Figure 9. The rogue waves are symmetrical about the coordinate plane.

9. Conclusions

In this paper, we used the proper transformations technique, bilinear equations, and HBM to examine several lump solution forms in a cascaded system with spatiotemporal dispersion and Kerr law nonlinearity. The vector-coupled nonlinear Schrödinger equation provides the mathematical model that describes how different solitons spread across a cascaded system. The lump solutions are assessed using the positive quadratic assumption in bilinear equations. We have created lump one soliton solutions for bilinear equations using a single exponential transformation. Using the double exponential transformation in the bilinear equation, we have calculated two lump soliton solutions. The evaluation of a mixed solution of lump waves and solitons is successful. Additionally,

by selecting appropriate trigonometric functions and hyperbolic functions, we have developed lump periodic solutions and rogue wave solutions. We also computed the stability of our solutions. The presented solutions have valuable uses in nonlinear optics and other areas. In future work, advanced techniques such as the bilinear neural network method and Lie symmetry analysis can be employed to explore and solve the governing model more efficiently.

Author contributions

Sarfaraz Ahmed: Methodology, investigation, conceptualization, software, writing original draft; Atef F. Hashem: Visualization, validation, writing review; Syed T. R. Rizvi: Supervision, methodology, investigation, conceptualization; Aly Seadawy: Supervision, projects, validation, sources. All authors have read and approved the final version of the manuscript for publication.

Use of Generative-AI tools declaration

The authors declare they have used Artificial Intelligence (AI) tools in the creation of this article.

Acknowledgments

This work was supported and funded by the Deanship of Scientific Research at Imam Mohammad Ibn Saud Islamic University (IMSIU) (grant number IMSIU-DDRSP2502).

Funding

This work was supported and funded by the Deanship of Scientific Research at Imam Mohammad Ibn Saud Islamic University (IMSIU) (grant number IMSIU-DDRSP2502).

Conflicts of interest

The authors declare no conflict of interest.

References

1. W. J. Liu, B. Tian, H. Q. Zhang, L. L. Li, Y. S. Xue, Soliton interaction in the higher-order nonlinear Schrödinger equation investigated with Hirota's bilinear method, *Phys. Rev. E*, **77** (2008), 066605. https://doi.org/10.1103/PhysRevE.77.066605
2. Z. D. Li, Q. Y. Li, X. H. Hu, Z. X. Zheng, Y. Sun, Hirota method for the nonlinear Schrodinger equation with an arbitrary linear time-dependent potential, *Ann. Phys.*, **332** (2007), 2545–2553. https://doi.org/10.1016/j.aop.2006.11.012
3. Y. Li, S. F. Tian, J. J. Yang, Riemann-Hilbert problem and interactions of solitons in the-component nonlinear Schrödinger equations, *Stud. Appl. Math.*, **148** (2022), 577–605. https://doi.org/10.1111/sapm.12450

4. Z. Q. Li, S. F. Tian, J. J. Yang, On the soliton resolution and the asymptotic stability of N-soliton solution for the Wadati-Konno-Ichikawa equation with finite density initial data in space-time solitonic regions, *Adv. Math.*, **409** (2022), 108639. https://doi.org/10.1016/j.aim.2022.108639
5. M. A. Banaja, A. A. Al Qarni, H. O. Bakodah, Q. Zhou, S. P. Moshokoa, A. Biswas, The investigate of optical solitons in cascaded system by improved adomian decomposition scheme, *Optik*, **130** (2017), 1107. https://doi.org/10.1016/j.ijleo.2016.11.125
6. S. T. Rizvi, A. R. Seadawy, S. Ahmed, K. Ali, Einstein's vacuum field equation: Lumps, manifold periodic, generalized breathers, interactions and rogue wave solutions, *Opt. Quant. Electron.*, **55** (2023), 181. https://doi.org/10.1007/s11082-022-04451-8
7. A. R. Seadawy, S. T. Rizvi, S. Ahmed, T. Batool, Propagation of W-shaped and M-shaped solitons with multi-peak interaction for ultrashort light pulse in fibers, *Opt. Quant. Electron.*, **55** (2023), 221. https://doi.org/10.1007/s11082-022-04478-x
8. A. R. Seadawy, S. Ahmed, S. T. Rizvi, K. Nazar, Applications for mixed Chen-Lee-Liu derivative nonlinear Schrödinger equation in water wave flumes and optical fibers, *Opt. Quant. Electron.*, **55** (2023), 34. https://doi.org/10.1007/s11082-022-04300-8
9. A. R. Seaway, S. T. Rizvi, A. Ahmad, S. Ahmed, Multiwave, rogue wave, periodic wave, periodic cross-lump wave, periodic cross-kink wave, lump soliton, breather lump, homoclinic breather, periodic cross-kink, M-shaped rational solutions and their interactions for the Degasperis-Procesi equation, *Int. J. Mod. Phys. B*, **13** (2023), 2350172. https://doi.org/10.1142/S0217979223501722
10. A. R. Seadawy, S. T. Rizvi, S. Ahmed, A. Ahmad, Study of dissipative NLSE for dark and bright, multiwave, breather and M-shaped solitons along with some interactions in monochromatic waves, *Opt. Quant. Electron.*, **54** (2022), 782. https://doi.org/10.1007/s11082-022-04198-2
11. S. Ahmed, A. R. Seadawy, S. T. Rizvi, Study of breathers, rogue waves and lump solutions for the nonlinear chains of atoms, *Opt. Quant. Electron.*, **54** (2022), 320. https://doi.org/10.1007/s11082-022-03732-6
12. K. Ali, A. R. Seadawy, S. Ahmed, S. T. Rizvi, Discussion on rational solutions for Nematicons in liquid crystals with Kerr Law, *Chaos. Soliton. Fract.*, **160** (2022), 112218. https://doi.org/10.1016/j.chaos.2022.112218
13. A. R. Seadawy, S. T. Rizvi, S. Ahmed, Weierstrass and Jacobi elliptic, bell and kink type, lumps, Ma and Kuznetsov breathers with rogue wave solutions to the dissipative nonlinear Schrödinger equation, *Chaos. Soliton. Fract.*, **160** (2022), 112258. https://doi.org/10.1016/j.chaos.2022.112258
14. A. R. Seadawy, S. Ahmed, S. T. Rizvi, K. Ali, Various forms of lumps and interaction solutions to generalized Vakhnenko Parkes equation arising from high-frequency wave propagation in electromagnetic physics, *J. Geom. Phys.*, **176** (2022), 104507. https://doi.org/10.1016/j.geomphys.2022.104507
15. A. R. Seadawy, S. Ahmed, S. T. Rizvi, K. Ali, Lumps, breathers, interactions and rogue wave solutions for a stochastic gene evolution in double chain deoxyribonucleic acid system, *Chaos. Soliton. Fract.*, **161** (2022), 112307. https://doi.org/10.1016/j.chaos.2022.112307
16. A. R. Seadawy, S. T. Rizvi, S. Ahmed, Multiple lump, generalized breathers, Akhmediev breather, manifold periodic and rogue wave solutions for generalized Fitzhugh-Nagumo equation: Applications in nuclear reactor theory, *Chaos. Soliton. Fract.*, **161** (2022), 112326. https://doi.org/10.1016/j.chaos.2022.112326

17. A. R. Seadawy, S. T. Rizvi, S. Ahmed, M. Younas, *Encyclopedia of complexity and systems science*, In: Applications of lump and interaction soliton solutions to the model of liquid crystals and nerve fibers, Berlin, Heidelberg: Springer, 2022, 1–20.
18. A. Bashir, A. R. Seadawy, S. Ahmed, S. T. Rizvi, The Weierstrass and Jacobi elliptic solutions along with multiwave, homoclinic breather, kink-periodic-cross rational and other solitary wave solutions to Fornberg Whitham equation, *Chaos. Soliton. Fract.*, **163** (2022), 112538. https://doi.org/10.1016/j.chaos.2022.112538
19. L. P. Aarts, P. V. D. Veer, Neural network method for solving partial differential equations, *Neural Process. Lett.*, **14** (2001), 261. https://doi.org/10.1023/A:1012784129883
20. R. F. Zhang, M. C. Li, Bilinear residual network method for solving the exactly explicit solutions of nonlinear evolution equations, *Nonlinear Dynam.*, **108** (2022), 521. https://doi.org/10.1023/A:1012784129883
21. X. R. Xie, R. F. Zhang, Neural network-based symbolic calculation approach for solving the Korteweg–de Vries equation, *Chaos. Soliton. Fract.*, **194** (2025), 116232. https://doi.org/10.1016/j.chaos.2025.116232
22. Q. S. Liu, Z. Y. Zhang, R. G. Zhang, C. X. Huang, Dynamical analysis and exact solutions of a new (2+1)-dimensional generalized Boussinesq model equation for nonlinear Rossby waves, *Commun. Theor. Phys.*, **71** (2019), 9. https://doi.org/10.5194/egusphere-2025-123
23. Q. Ouyang, Z. Zhang, Q. Wang, W. Ling, P. Zou, X. Li, Solitary, periodic, kink wave solutions of a perturbed high-order nonlinear Schrödinger equation via bifurcation theory, *Propuls. Power. Res.*, **130** (2024), 1107. https://doi.org/10.1016/j.jppr.2024.07.001
24. U. Younas, M. Younis, A. R. Seadawy, S. T. R. Rizvi, S. Althobaiti, S. Sayed, Diverse exact solutions for modified nonlinear Schrödinger equation with conformable fractional derivative, *Results Phys.*, **20** (2021), 103766. https://doi.org/10.1016/j.rinp.2020.103766
25. U. Akram, A. R. Seadawy, S. T. R. Rizvi, M. Younis, S. Althobaiti, S. Sayed, Traveling wave solutions for the fractional Wazwaz–Benjamin–Bona–Mahony model in arising shallow water waves, *Results Phys.*, **20** (2021), 103725. https://doi.org/10.1016/j.rinp.2020.103725
26. A. R. Seadawy, M. Bilal, M. Younis, S. T. R. Rizvi, S. Althobaiti, M. M. Makhlouf, Analytical mathematical approaches for the double-chain model of DNA by a novel computational technique, *Chaos. Soliton. Fract.*, **144** (2021), 110669. https://doi.org/10.1016/j.chaos.2021.110669
27. A. R. Seadawy, S. U. Rehman, M. Younis, S. T. R. Rizvi, S. Althobaiti, M. M. Makhlouf, Modulation instability analysis and longitudinal wave propagation in an elastic cylindrical rod modelled with Pochhammer-Chree equation, *Phys. Scripta*, **96** (2021), 045202. https://doi.org/10.1088/1402-4896/abdcf7
28. A. R. Seadawy, S. T. R. Rizvi, S. Ahmad, M. Younis, D. Baleanu, Lump, lump-one stripe, multiwave and breather solutions for the Hunter–Saxton equation, *Open Phys.*, **96** (2021), 10. https://doi.org/10.1515/phys-2020-0224
29. M. Bilal, A. R. Seadawy, M. Younis, S. T. R. Rizvi, K. E. Rashidy, S. F. Mahmoud, Analytical wave structures in plasma physics modelled by Gilson-Pickering equation by two integration norms, *Results Phys.*, **23** (2021), 103959. https://doi.org/10.1016/j.rinp.2021.103959
30. S. T. R. Rizvi, A. R. Seadawy, M. Younis, I. Ali, S. Althobaiti, S. F. Mahmoud, Soliton solutions, Painleve analysis and conservation laws for a nonlinear evolution equation, *Results Phys.*, **23** (2021), 103999. https://doi.org/10.1016/j.rinp.2021.103999

31. S. T. R. Rizvi, A. R. Seadawy, M. Younis, S. Iqbal, S. Althobaiti, A. M. E. Shehawi, Various optical soliton for a weak fractional nonlinear Schrödinger equation with parabolic law, *Results Phys.*, **23** (2021), 103998. https://doi.org/10.1016/j.rinp.2021.103998
32. A. R. Seadawy, S. T. Rizvi, I. Ali, M. Younis, K. Ali, M. M. Makhlouf, et al., Conservation laws, optical molecules, modulation instability and Painlevé analysis for the Chen–Lee–Liu model, *Opt. Quant. Electron.*, **23** (2021), 15. https://doi.org/10.1007/s11082-021-02823-0
33. K. U. Tariq, H. Zainab, A. R. Seadawy, M. Younis, S. T. R. Rizvi, A. M. A. Allah, On some novel optical wave solutions to the paraxial M-fractional nonlinear Schrödinger dynamical equation, *Opt. Quant. Electron.*, **23** (2021), 14. https://doi.org/10.1007/s11082-021-02855-6
34. S. Ahmed, R. Ashraf, A. R. Seadawy, S. T. R. Rizvi, M. Younis, A. Althobaiti, et al., Lump, multi-wave, kinky breathers, interactional solutions and stability analysis for general (2 + 1)-rth dispersionless Dym equation, *Results Phys.*, **23** (2021), 104160. https://doi.org/10.1016/j.rinp.2021.104160
35. M. Bilal, A. R. Seadawy, M. Younis, S. T. R. Rizvi, H. Zahed, Dispersive of propagation wave solutions to unidirectional shallow water wave Dullin–Gottwald–Holm system and modulation instability analysis, *Math. Method. Appl. Sci.*, **44** (2021), 4104. https://doi.org/10.1016/j.padiff.2022.100444
36. M. Younis, A. R. Seadawy, M. Bilal, S. T. R. Rizvi, S. Althobaiti, M. Alkafafy, Nonlinear dynamical wave structures to the Date–Jimbo–Kashiwara–Miwa equation and its modulation instability analysis, *Mod. Phys. Lett. B*, **35** (2021), 2150300. https://doi.org/10.1016/j.aml.2024.109348
37. S. Ahmed, A. M. Mubaraki, Pulse-driven robot: Motion via distinct lumps and rogue waves, *Opt. Quant. Electron.*, **65** (2024), 225. https://doi.org/10.1007/s11082-023-05816-3
38. A. R. Seadawy, S. U. Rehman, M. Younis, S. T. R. Rizvi, S. Althobaiti, M. M. Makhlouf, Modulation instability analysis and longitudinal wave propagation in an elastic cylindrical rod modelled with Pochhammer-Chree equation, *Phys. Scripta*, **96** (2021), 045202. https://doi.org/10.1088/1402-4896/abdcf7
39. Y. Liu, B. Li, A. M. Wazwaz, Novel higher order breathers and rogue waves in the Boussinesq equation via determinants, *Int. J. Mod. Phys. B*, **43** (2020), 3715. https://doi.org/10.1002/mma.6148
40. K. L. Geng, D. S. Mou, C. Q. Dai, Nondegenerate solitons of 2-coupled mixed derivative nonlinear Schrödinger equations, *Nonlinear Dynam.*, **111** (2023), 617. https://doi.org/10.1016/j.physleta.2019.126201
41. J. J. Fang, D. S. Mou, H. C. Zhang, Y. Y. Wang, Discrete fractional soliton dynamics of the fractional Ablowitz-Ladik model, *Optik*, **228** (2021), 166186. https://doi.org/10.1016/j.ijleo.2020.166186
42. W. B. Bo, R. R. Wang, Y. Fang, Y. Y. Wang, C. Q. Dai, Prediction and dynamical evolution of multipole soliton families in fractional Schrödinger equation with the PT-symmetric potential and saturable nonlinearity, *Nonlinear Dynam.*, **111** (2023), 1588. https://doi.org/10.1007/s11071-022-07884-8
43. X. Wen, R. Feng, J. Lin, W. Liu, F. Chen, Q. Yang, Distorted light bullet in a tapered graded-index waveguide with PT symmetric potentials, *Optik*, **248** (2021), 168092. https://doi.org/10.1016/j.ijleo.2021.168092

44. R. R. Wang, Y. Y. Wang, C. Q. Dai, Influence of higher-order nonlinear effects on optical solitons of the complex Swift-Hohenberg model in the mode-locked fiber laser, *Opt. Laser. Technol.*, **152** (2022), 108103. https://doi.org/10.1016/j.optlastec.2022.108103
45. H. Y. Wu, L. H. Jiang, One-component and two-component Peregrine bump and integrated breather solutions for a partially nonlocal nonlinearity with a parabolic potential, *Optik*, **262** (2022), 169250. https://doi.org/10.1016/j.ijleo.2022.169250
46. Y. Fang, G. Z. Wu, X. K. Wen, Y. Y. Wang, D. D. Dai, Predicting certain vector optical solitons via the conservation-law deep-learning method, *Opt. Laser. Technol.*, **155** (2022), 108428. https://doi.org/10.1016/j.optlastec.2022.108428
47. S. T. Rizvi, A. R. Seadawy, S. Ahmed, F. Ashraf, Novel rational solitons and generalized breathers for (1+1)-dimensional longitudinal wave equation, *Mod. Phys. Lett. B*, **37** (2023), 2350269. https://doi.org/10.1142/S0217979223502697
48. Q. Zhou, Q. Zhu, H. Yu, Y. Liu, C. Wei, P. Yao, et al., Bright, dark and singular optical solitons in a cascaded system, *Laser Phys.*, **25** (2014), 025402. https://doi.org/10.1088/1054-660X/25/2/025402
49. X. Zhang, Q. C. Zhong, V. Kadirkamanathan, J. He, J. Huang, Source-side series-virtual-impedance control to improve the cascaded system stability and the dynamic performance of its source converter, *IEEE T. Power. Electr.*, **34** (2018), 5866. https://doi.org/10.1109/TPEL.2018.2867272
50. M. A. Banaja, A. A. A. Qarni, H. O. Bakodah, Q. Zhou, S. P. Moshokoa, A. Biswas, The investigate of optical solitons in cascaded system by improved adomian decomposition scheme, *Optik*, **130** (2019), 1114. https://doi.org/10.1016/j.ijleo.2016.11.125
51. A. Sonmezoglu, M. Ekici, M. Mirzazadeh, Q. Zhou, M. F. Mahmood, E. Zerrad, et al., Optical solitons in cascaded system by extended trial function method, *J. Comput. Theor. Nanos.*, **13** (2016), 5398. https://doi.org/10.1166/jctn.2016.5429
52. N. Raza, A. Jhangeer, S. Arshed, M. Inc, The chaotic, supernonlinear, periodic, quasiperiodic wave solutions and solitons with cascaded system, *Wave Random Complex*, **13** (2021), 15. https://doi.org/10.1080/17455030.2021.1945164
53. A. R. Seadawy, S. T. Rizvi, M. A. Ashraf, M. Younis, M. Hanif, Rational solutions and their interactions with kink and periodic waves for a nonlinear dynamical phenomenon, *Mod. Phys. Lett. B*, **35** (2021), 2150236. https://doi.org/10.1142/S0217979221502362
54. H. Wang, Lump and interaction solutions to the (2 + 1)-dimensional Burgers equation, *Appl. Math. Lett.*, **85** (2018), 34. https://doi.org/10.1016/j.aml.2018.05.010
55. Y. Zhou, S. Manukure, W. X. Ma, Lump and lump-soliton solutions to the Hirota Satsuma equation, *Commun. Nonlinear Sci.*, **68** (2019), 62. https://doi.org/10.1016/j.cnsns.2018.07.038
56. P. Wu, Y. Zhang, I. Muhammad, Q. Yin, Lump, periodic lump and interaction lump stripe solutions to the (2 + 1)-dimensional B-type Kadomtsev–Petviashvili equation, *Mod. Phys. Lett. B*, **32** (2018), 1850106. https://doi.org/10.1142/S0217984918501063
57. B. Q. Li, Y. L. Ma, Multiple-lump waves for a (3 + 1)-dimensional Boiti–Leon–Manna–Pempinelli equation arising from incompressible fluid, *Comput. Math. Appl.*, **76** (2018), 214. https://doi.org/10.1016/j.camwa.2018.04.015
58. M. M. Khater, Computational simulations; propagation behavior of the Riemann wave interacting with the long wave, *J. Ocean Eng. Sci*, **342** (2023), 453. https://doi.org/10.1016/j.joes.2022.05.022

59. R. Hirota, Exact solution of the Korteweg-de Vries equation for multiple collisions of solitons, *Phys. Rev. Lett.*, **27** (1971), 1192. https://doi.org/10.1103/PhysRevLett.27.1192

AIMS Press